

The author(s) shown below used Federal funds provided by the U.S. Department of Justice and prepared the following final report:

Document Title: Development of a Surrogate Bruising Detection System to Describe Bruising Patterns Associated with Common Childhood Falls, Final Report

Author(s): Gina Bertocci, Ph.D., P.E., Raymond Dsouza, M.S.

Document No.: 242018

Date Received: April 2013

Award Number: 2008-DD-BX-K311

This report has not been published by the U.S. Department of Justice. To provide better customer service, NCJRS has made this Federally-funded grant report available electronically.

Opinions or points of view expressed are those of the author(s) and do not necessarily reflect the official position or policies of the U.S. Department of Justice.

Development of a Surrogate Bruising Detection System to Describe Bruising Patterns Associated with Common Childhood Falls

Submission Date: Nov, 2012

Grant No.: 2008-DD-BX-K311

Authors:

1) Gina Bertocci, PhD, PE (Principal Investigator)
University of Louisville
Dept of Mechanical Engineering
Rm 204, Health Sciences Research Tower
500 S. Preston St.
Louisville, KY 40202
502.852.0296 g.bertocci@louisville.edu

2) Raymond Dsouza, MS
University of Louisville
Dept of Mechanical Engineering
Rm 110, Instructional Building
500 S. Preston St.
Louisville, KY 40202
502.852.0279 rz.zray@gmail.com

This project was supported by Grant No. 2008-DD-BX-K311 awarded by the National Institute of Justice, Office of Justice Programs, US Department of Justice. Points of view in this document are those of the authors and do not necessarily represent the official position or policies of the US Department of Justice.

Abstract

Background:

Child abuse is a leading cause of fatality in children 0-4 years of age. Roughly 1500 children are fatally abused each year. Many serious injuries and fatalities could have been prevented if clinicians and child protective services were able to better distinguish between injuries associated with abuse and those caused by accidents. Clinicians, child protective services and law enforcement personnel must therefore be equipped with knowledge related to the types of injuries that are possible from common household accidents that are often reported to be the underlying cause of injury in child abuse. The ability to detect child abuse at the earliest stages has proven critical in the prevention of escalating injury severity and even death. Bruising is an early sign of abuse, and can be an effective indicator or sentinel of child abuse. Moreover, bruising patterns can provide a “roadmap” documenting a child’s exposure to impact or contact. Clinical studies have demonstrated that bruising characteristics differ in children exposed to abusive vs. accidental trauma.

Our previous research has relied upon the use of instrumented anthropomorphic test devices (i.e. test dummies or human surrogates) to investigate injury risk in common childhood falls. However, existing test dummies do not have the capability of predicting soft tissue injury or potential bruising patterns; this capability could prove useful in the distinction between abusive and accidental injuries.

Research Goals and Objectives:

Our goal was to design and develop a prototype surrogate bruising detection device having the capability to predict potential bruising patterns in children when adapted to a test dummy used to simulate common household fall events often stated as false scenarios in child abuse¹. The scope of

our project included the development of a “sensing skin” that can be adapted to a commercial test dummy representing a 12 month old child, along with a data acquisition system and software capable of displaying sensor output and location on a 3D representation of a human surrogate. When used in future mock laboratory experiments, the sensing skin-adapted test dummy will have the capability of measuring and recording levels of impact force, documenting the locations of impact on the test dummy, and representing the number of impact points encountered.

Research Design and Methodology

Matrices of individual force sensing resistive sensors were designed and fabricated in-house to adapt to each body segment of the test dummy. These sensor matrices were enveloped between neoprene layers to form sensing skins. Data from the sensors were acquired through our custom-designed data acquisition system and compiled in a computerized 3D visual body map image capable of displaying the areas of contact or impact that represent potential bruising or soft tissue injury. This body map image will provide a “roadmap” of the child surrogate’s contact exposure during a specific event.

Research Results and Conclusions

The primary outcome of our project is a prototype surrogate bruising detection device that includes: 1) custom-designed, low-cost force sensors that are integrated into matrices incorporated into a “skin” that adapts to a commercial 12 month old test dummy, 2) a data acquisition system that can capture and record force sensor output and location during a simulated fall or other event, 3) a computerized body mapping system that displays color-coded sensor output indicating the level of applied force to specific body regions, along with the location of force application. Our prototype surrogate bruising

detection system will be capable of predicting potential bruising numbers, patterns and location when adapted to a child test dummy used in simulations of falls or other events.

¹ - utility patent application no. US 2008/0289438 pending - submitted May 21, 2008

Table of Contents

Executive Summary.....	6
I. Introduction.....	10
1. Statement of the problem	10
2. Literature citations and review	10
3. Statement of hypothesis or rationale for research.....	18
II. Methods	19
Sensor Evaluation	20
Sensing Skin.....	22
Data Acquisition System.....	23
Evaluation of Sensing Skin Prototypes	23
Extend Sensing Skin to Entire ATD	24
III. Results	24
Sensor Evaluation	24
In-House Integrated Sensor Matrix Design and Fabrication	26
Forearm Sensing Skin Prototypes	30
Data Acquisition System.....	31
Extend Sensing Skin to Entire ATD	33
IV. Conclusions.....	34
Discussion of Findings	34
Limitations.....	36
Implications for Policy and Practice	38
Implications for Further Research.....	39
V. References.....	40
Appendix A – FSR Sensor Manufacturer Specifications and Design Criteria.....	44
Appendix B – Static Loading Characterization of Commercial FSR Sensors.....	46
Appendix C – Impact Testing of Commercial Sensors and In-House Milled Sensors.....	54
Appendix D – Photolithographic Process to Generate Integrated Sensor Matrix.....	56
Appendix E – In-House Printed Sensor Performance vs. Design Criteria.....	62
Appendix F – Sensor Matrix Designs for Various ATD Body Regions	63

Executive Summary

Child abuse is a leading cause of trauma-related fatality in children 0-4 years of age [DHHS, 2006]. Roughly 1500 children are fatally injured each year in association with child abuse and 150,000 are permanently disabled [DHHS, 2006]. Fatalities were greatest amongst children 1 year of age and younger. Many serious injuries and fatalities could have been prevented if clinicians and child protective services were able to better distinguish between those injuries associated with abuse and those injuries caused by accidents. Clinicians, child protective services and law enforcement personnel would greatly benefit from knowledge related to the types of injuries that are truly possible from common household accidents often reported to be the underlying cause of injury in child abuse. Knowledge of the type of injuries that can result from common household accidents can equip personnel responsible for distinguishing between abusive and accidental injuries with information that is key to decision-making. Although not life threatening injuries, bruising patterns provide a “roadmap” documenting a child’s exposure to violence or a simple childhood fall. That is, for each and every substantial impact to the child’s body, a resulting soft tissue injury will likely develop. Previous studies have shown that bruising patterns resulting from abuse are significantly different than those resulting from accidents [Atwal, 1998; Dunstan, 2002; Pierce, 2010]. This distinguishing feature of abuse is often overlooked in the clinical setting, as well as in forensic investigations. In a forensic investigation of physical child abuse, a child’s bruising “roadmap” can permit engineers to evaluate the compatibility of the biodynamics of the stated cause (e.g. stairfall or bed fall) and the presenting soft tissue injuries. Failure to verify biodynamic compatibility between the bruising pattern and stated cause should raise questions regarding the veracity of the provided history. It is this evaluation of biodynamic compatibility based upon the bruising “roadmap” that our study aimed to address.

Our long-term goal was to develop a forensic tool that can be used to delineate between child abuse and accidents based upon presenting bruising patterns. Our project goal was to design and develop a prototype surrogate bruising detection system capable of capturing and recording potential bruising patterns that occur in child surrogates when used in simulated household fall events often stated as false histories in child abuse. Since children 1 year of age and younger experience increased abusive fatality rates, our bruising detection system was designed for use with a surrogate representing a 1-year-old child. This forensic tool will ultimately be utilized to develop a knowledge base of bruising “roadmaps” that are associated with common childhood fall events. The data generated from use of our system could also aid in assessment of events stated as causes of bruising in specific child abuse forensic investigations. (US Patent No. US 2008/0289438 pending)

Our approach consisted of 1) designing and fabricating customized force sensors that can be of varying sizes and arranged in matrices contouring to the various segments of a pediatric anthropomorphic test device (ATD), 2) designing and developing a prototype force sensing skin that was adapted to the ATD forearm, 3) designing and developing a prototype data acquisition system that collected and compiled sensor output data from the ATD forearm, 4) designing and developing a prototype computerized visual body mapping system capable of displaying impact force application and corresponding locations and patterns of potential bruising on the ATD forearm, 5) integrating and demonstrating functionality of the surrogate bruising detection system consisting of the prototype forearm sensing skin adapted to the ATD, data acquisition system and computerized body (forearm) mapping image system, and 6) extending the prototype surrogate bruising detection system to the entire ATD.

In our study we designed and developed a surrogate bruising detection system that can be used to predict and investigate potential bruising patterns in simulated falls or events involving children. The system consists of 1) custom-designed, low-cost pressure sensors that are integrated into matrices incorporated into a “skin” that adapts to a commercial 1-year-old ATD (CRABI ATD), 2) a data acquisition system capable of capturing and recording force sensor output and location during a simulated fall or other event, 3) a computerized body mapping system that displays color-coded sensor output indicating the level of applied force to specific body regions. Our surrogate bruising detection system will be capable of predicting potential bruising numbers, patterns and location when adapted to a 1-year-old ATD used in simulations of falls or other events. It is important to note that our system indicates *bruising potential*, and does not definitively indicate whether a bruise would occur or not given variations in bruising thresholds across individuals. Our bruising detection system is limited by the biofidelity of the ATD (how “human-like”) to which it is applied. For example, material representing the ATD soft tissue may not possess the same biomechanical properties of human soft tissue, thus influencing the measured force application to a specific region of the ATD body. Moreover, movement or dynamics of the ATD during a fall are typically dependent upon joint biomechanical properties; in relatively low speed events such as falls, the CRABI ATD joint responses may not be consistent with those of a human child. Such differences can influence fall dynamics, and thus predicted bruising patterns.

The surrogate bruising detection system can aid in the overall assessment of whether a child’s injury was a result of abusive or accidental trauma. The surrogate bruising detection system has the potential to influence child abuse diagnosis, investigations, and prosecution by providing objective data regarding bruising patterns. (Similarly, this data can also aid in the exoneration of caregivers who are

innocent of inflicting physical abuse.) In the diagnosis, investigation and legal prosecution of child abuse cases, bruising patterns are often disregarded by pediatricians, child protective services, law enforcement personnel, biomechanics experts, and the judicial system given that these injuries are typically non-life threatening. However, ignoring the presence of bruising patterns is a missed opportunity to gain a better understanding of the environment that a child has been exposed to since bruising provides a “roadmap” of the child’s exposure to force application.

Bruising patterns are critical to biomechanical expert witness testimony in child injury litigation, providing key evidentiary data in the assessment of biodynamic compatibility of a stated cause and resulting injuries. The cumulative number of bruises and their location has been shown to aid in the discrimination between abuse and accident in children. Use of our device is expected to provide clinicians, child protective services, law enforcement personnel, biomechanical experts, and judiciary personnel with objective data as to the bruising patterns that can be expected in common household accidents that are often provided as false histories in an effort to conceal child abuse. Conversely, use of the surrogate bruising detection system in its ability to provide objective data regarding bruising patterns can also serve to exonerate those who are innocent of alleged abuse. In summary, the surrogate bruising detection system can provide an objective method to elucidate the differences in bruising patterns that may occur in abusive vs. accidental trauma to aid in the diagnosis and prosecution of child abuse.

This project was supported by Grant No. 2008-DD-BX-K311 awarded by the National Institute of Justice, Office of Justice Programs, US Department of Justice. Points of view in this document are those of the authors and do not necessarily represent the official position or policies of the US Department of Justice.

I. Introduction

1. Statement of the problem

Early detection of child abuse may prevent repeat, escalating injury in a child, and can provide an opportunity for further clinical evaluation or intervention. Although bruising is one of the most common injuries associated with child abuse [Lynch 1975; Smith 1974], it is also commonly found in accidental injury as well. A number of studies have demonstrated that bruising characteristics differ across accidents vs. abuse [Dunstan 2002; Pierce 2010]. Knowledge of bruising patterns that can result from common household accidents, often falsely reported in child abuse, can equip those responsible for distinguishing between abusive and accidental injuries with information that is key to decision-making critical to a child's health and safety. Our goal was to design and development a prototype surrogate bruising detection system capable of describing potential bruising patterns that occur in child surrogates when used in simulated household fall events often stated as false histories in child abuse.

2. Literature citations and review

Child Abuse Statistics

In 2006, there were 3.573 million reports of child maltreatment made to Child Protective Services, with 910,000 indicated cases of child abuse or neglect [DHHS, 2006]. In the US, between 1500-5000 children die and 150,000 children are seriously injured from child abuse and neglect each year [DHHS, 2006; Herman-Giddens, 1999]. According to the National Child Abuse and Neglect Data System, in 2006 more than 78% of abuse fatalities occurred in children less than 4 years old [DHHS, 2006]. Abuse is the leading cause of fatalities due to trauma in children < 4 years of age, causing more deaths than motor vehicle crashes and drowning combined [DHHS, 2006]. Fatalities were greatest amongst children 1 year of age and younger. As noted in Healthy People 2010, child maltreatment and associated fatalities

remain a significant cause of morbidity and mortality in young children [DHHS, 2000]. Additionally, the direct and indirect costs of child abuse in the US are staggering, with estimates nearing \$258 million per day [America, 2008]. Direct costs include health care services, child welfare services, law enforcement services and judicial system costs. Indirect costs associated with child abuse include those associated with special education, mental health care, continued health care, and lost productivity to society. These costs translate to roughly \$1,462 per US family, with annualized costs estimated as high as \$104 billion per year.

Failure to Diagnose Child Abuse

Many of the 1500 children that die each year due to child abuse are seen at medical facilities for their injuries prior to death, but early signs of abuse are often missed or dismissed. Repeat injury is likely, with 50-80% of fatal or near-fatal abuse cases having evidence of prior injuries [Alexander, 1990; Jenny, 1999]. Bruising is common in child abuse, but is often missed as an indicator given its clinical insignificance. Pierce et al. found that bruising was missed in roughly 44% of fatal or near-fatal cases [Pierce, 2010]. Providing front-line pediatricians and clinicians with knowledge of abusive vs. non-abusive bruising patterns could aid in reducing missed cases of abuse. Use of the surrogate bruising detection system to develop a knowledge base of bruising “roadmaps” will provide a step towards achieving this goal.

Failure to Prosecute Substantiated Child Abuse Cases

Of the 3.573 million reports of child abuse to Child Protective Services, 61.7% received further screenings, and 910,000 cases were substantiated [DHHS, 2006]. However, the number of substantiated cases of child abuse that result in criminal prosecution are substantially fewer in number [Cross, 2003; Sedlak, 2006]. Reasons for not filing criminal charges include the need for further investigation, insufficient evidence and victim issues related to age, willingness to testify and unknown

location. Tjaden et al. found that of 833 substantiated child maltreatment cases only 21% resulted in dependency court filings and 4% in criminal court filings [Tjaden, 1992]. Cross et al. conducted a meta-analysis of 21 studies of child abuse prosecution and found that “most substantiated and founded child abuse cases do not lead to prosecution, but the majority of cases that are prosecuted do end in conviction” [Cross, 2003]. Recently, Sedlack et al. followed the justice system path of 225 child abuse cases investigated by Child Protective Services [Sedlak, 2006]. 210 of these cases were referred to law enforcement (93%) for criminal investigation of which 160 cases (71%) were opened for investigation; the remaining 50 cases were dropped by law enforcement or were of unknown status. Thirty-six (36%) percent (n=81) of the investigated cases led to sheriff arrests, while 89 (40%) of the cases were sent on for prosecution. Of these 81 cases, 72 were filed as felonies, 10 were filed as misdemeanors and 7 received no filing. Of the felony and misdemeanor cases filed, 33% of the perpetrators pled guilty, 10% of the cases were “nol-pros” dismissals, and in 8% of the cases there was a “no contest” plea. Overall, 147 cases (65%) led to criminal charges.

Bruising in Children Associated with Accidents and Abuse

Bruising is one of the most common outcomes of abuse [Lynch, 1975; Smith, 1974]. Although not a life-threatening injury, bruising can be an early indicator of abuse that is easily recognized without the need for diagnostic tests. Despite providing a “roadmap” describing the environment that a child has been exposed to, bruising is often ignored in the assessment of a child’s injuries when attempting to differentiate between abusive and non-abusive injuries. Failure to properly interpret the indications provided by bruising patterns can result in a child being returned to an unsafe environment where repeat abuse may occur.

The scientific literature provides strong evidence that differences in bruising patterns (location, number, size) exist in children exposed to accidents vs. those exposed to physically abusive conditions. Maguire [Maguire, 2005] compiled evidence in support of this hypothesis in his comprehensive review of the scientific literature to determine whether patterns of bruising in childhood are diagnostic or suggestive of abuse. In doing so, Maguire reviewed the scientific literature related to bruising associated with accidents, as well as bruising patterns associated with abuse. Key studies, as well as Maguire's conclusions are described below.

Bruising Associated with Accidents – Maguire [Maguire, 2005] identified seven studies [Carpenter, 1999; Dunstan, 2002; Labbe, 2001; Mortimer, 1983; Sugar, 1999; Tush, 1982] meeting inclusion criteria that addressed bruising patterns in non-abused children. Some of the key findings of these studies, along with others include:

- Increased bruising was noted in the summer [Labbe, 2001]
- Increased bruising was noted with increased family size [Carpenter, 1999]
- Bruises were characteristically small [Carpenter, 1999; Mortimer, 1983; Dunstan, 2002]
- Prevalence and mean number of bruises increased with age and developmental stage [Sugar, 1999; Carpenter, 1999; Labbe, 2001]
- Bruising in a child who has no independent mobility was very uncommon [Carpenter, 1999; Sugar, 1999]
- Most common sites of bruising in children who are walking are the knees and shins [Sugar, 1999; Tush, 1982; Wedgewood, 1990]
- Bruises occurred over bony prominences [Sugar, 1999; Carpenter, 1999]

- Bruising was uncommon to the back, buttocks, forearm, face, abdomen or hip, upper arm, posterior leg or foot in children of any developmental stage [Sugar, 1999; Carpenter, 1999; Tush, 1982; Wedgewood, 1990]
- Bruising to the ears [Dunstan, 2002] and hands (all 7 studies) did not occur
- Children in intensive care due to accidental causes had a median of 1.5 bruises, with a total of 4 or fewer bruises [Pierce, 2010]
- Children in intensive care due to accidental causes had no bruising to the ear, neck, hands, chest, buttocks, genitourinary area or hip regions [Pierce, 2010]

Bruising Associated with Abuse – Maguire [2005] also described studies focusing primarily on bruising in abused children. Key findings of these studies, as well as a study by Pierce et al., are as follows:

- Bruises are common in child abuse
- Mean number of bruises in abused children varied from 5.7 to 10, while controls have a mean number of 1.5 [Atwal, 1998; Dunstan, 2002]
- Measured length of bruises was greater in abused children [Dunstan, 2002]
- The head was the most common site of bruising in abused children [de Silva, 1993; Dunstan, 2002; Smith, 1974; Worlock, 1986]
- Multiple bruises to the head and face were found to occur in fatal child abuse cases [de Silva, 1993]
- Bruising to the ear, face, head, neck, trunk, buttocks and arms is seen significantly more in abused children than controls [Dunstan, 2002; Atwal, 1998]
- Bruising to children with abusive fractures were found to the head and neck [Worlock, 1986]

- In contrast to non-abused children, bruises were found to non-bony prominence areas [Naidoo, 2000]
- A common feature in abused children was clustering of bruises [Barlow, 1983; Sussman, 1968]. The bruises were thought to be associated with a defensive maneuver and were often found on the arm, thigh and trunk.
- Bruises often carried the imprint of an implement used to inflict injury [Brinkman, 1979; Sussman, 1968]
- Children in intensive care due to abusive causes had a median of 6 bruises, with up to as many as 25 bruises [Pierce, 2010]
- Children in intensive care due to abusive causes were found to have bruising to the ear, neck, hands, right arm, chest, buttocks, genitourinary area, and hip regions [Pierce, 2010]

Collectively these studies strongly suggest that bruising patterns associated with child abuse differ substantially from those occurring as a result of an accident in terms of body region affected, number of bruises, and size of bruises. Age of the child and developmental stage are also important factors that must contribute to determining whether bruising is associated with abusive or accidental trauma. Given these differences, it is reasonable to assert that bruising patterns can be used as an indicator in attempting to differentiate between abuse and accidental trauma. One study that attempted to quantify this difference was conducted by Dunstan [2002] and is described below.

Dunstan et al. found a significant difference in the number of bruises across all body regions when comparing children injured through abuse to those injured in accidents [Dunstan, 2002]. 763 bruises were found in 133 abused children, while 282 bruises were found in 189 control children in this study.

There were clear statistical differences in the number of bruises present in abused vs. non-abused children for all body regions except for the legs. Dunstan also investigated location of bruising in his study and found that bruising to the head and neck was common in abused children, but rare in children that had been accidentally injured. Dunstan further determined that head and neck bruises in victims subjected to accidental trauma were no larger than 0.1 cm in mean total length, whereas abused children were found to have head and neck bruises of a mean total length of 5.1 cm. Dunstan concluded, “the extent of bruising tends to be a good discriminator between children that were abused and those who were not.” Dunstan also found ear bruising to be an indicator of abuse in his study of 133 abused children and 189 control children. Ear bruising was present in 16 percent of abused children, but not present in any of the control children in his study resulting in a statistically significant difference [Dunstan, 2002]. Similarly, Pierce et al. found 16% of children (age 0-48 months) in intensive care with abusive trauma to have ear bruising [Pierce, 2010]. Bruising of the external ear (auricle) is an uncommon accidental injury and is a marker of severe injury in children admitted to the hospital as a result of an abusive injury [Herr, 2003a]. Herr et al. documented that bruising of the external ear occurred in 22% of children admitted to the hospital as a result of abusive injury, and was present in 6 of 9 children who died from abusive trauma. Herr also found that children with abusive injury who presented with external ear bruising had at least one other region of bruising, and that bruising is more frequently present in abuse victims who are > 1 year of age [Herr, 2003b].

Use of Anthropomorphic Test Devices (ATDs) in Child Abuse Research

In the recent past Anthropomorphic Test Devices (ATD), often referred to as crash test dummies or human surrogates, have been used to study pediatric falls, as well as shaken baby syndrome [Bertocci, 2003; Bertocci, 2004; Cory, 2003; Deemer, 2005; Duhaime, 1987; Thompson, 2009; Thompson 2012;

Prange, 2003]. In the absence of human volunteers, these surrogates provide a means of estimating injury risk and understanding injury mechanisms associated with various potentially injurious events. Our lab has conducted a number of pediatric ATD studies simulating free falls and bed falls to investigate the potential for fractures and head injury [Bertocci, 2003; Bertocci, 2004; Deemer, 2005; Thompson, 2009; Thompson 2012]. Our experimental studies have utilized ATDs representing both 12 month old (CRABI ATD) and 3 year old (Hybrid II and III ATD) children. One of the first human surrogate studies in the child abuse field was conducted by Duhaime who investigated shaking baby syndrome using a modified doll [Duhaime, 1987] to represent an infant. Prange et al. investigated free falls using a customized infant surrogate, but additionally studied inflicted impacts to the head and repeated Duhaime's shaking baby experiments [Prange, 2003]. Recently, Jenny has developed a highly biofidelic (human-like) infant surrogate that was used to study a variety of injurious events (e.g. inflicted head impact) that might be encountered in an abusive environment [Jenny, 2006]. Despite limitations in ATD biofidelity that may exist, these studies have allowed for comparative analyses of injury scenarios (e.g. shaking vs. free fall) to assess relative risk of injury. However, limitations in ATD biofidelity must be considered when drawing conclusions from these experimental studies. Use of ATD experiments has also begun to find its way into the judicial system, with biomechanics experts conducting ATD experiments to evaluate injury risk associated with possible injury scenarios in alleged child abuse cases. With the introduction of biomechanics experts testifying in child abuse cases, it is expected that the use of ATDs or human surrogates to study injury potential in alleged child abuse will greatly increase.

Forensic Investigations of Alleged Child Abuse – Utility of Biomechanics

Traditionally, the determination of whether a child's injuries were inflicted or the result of an accident fell solely on the attending or primary care physician. However, more recently bioengineers with expertise in injury biomechanics have been called upon to serve as part of multi-discipline child advocacy teams, as well as to testify as expert witnesses. Bioengineers are typically trained in engineering principles and life sciences making them uniquely qualified to study injury mechanisms, injury thresholds, injury risk, etc. associated with a variety of events including vehicle crashes and falls. A forensic investigation conducted by bioengineers will often include attempting to reconstruct the dynamics of an event to verify that presenting injuries are compatible [Coghlan, 2005; Hayes, 2007]. Investigations may rely upon a combination of manual calculations, computer simulation, and/or experiments using human surrogates to estimate the injury potential associated with a specific event [Bertocci, 2006; Pierce, 2008]. It is anticipated that biomechanical analysis included as a part of forensic child abuse investigations will continue to grow, providing an increased level of scientific evidence.

3. Statement of hypothesis or rationale for research

Our study focused on the design and development of a new technology, and thus was not a hypothesis-driven study. Our study goal was to design and develop a prototype surrogate bruising detection system capable of characterizing potential bruising patterns that occur in child surrogates used to simulate household fall events that are often stated as false histories in child abuse. This forensic investigative tool will ultimately be utilized to develop a knowledge base of bruising "roadmaps" that are associated with common childhood fall events. The system could also be employed to explore potential bruising patterns associated with events stated as causes of injury in specific child abuse forensic investigations.

II. Methods

The surrogate bruising detection system conceptual model consisted of an adapted sensing skin, data acquisition system, and computerized body mapping image system (Figure 1).

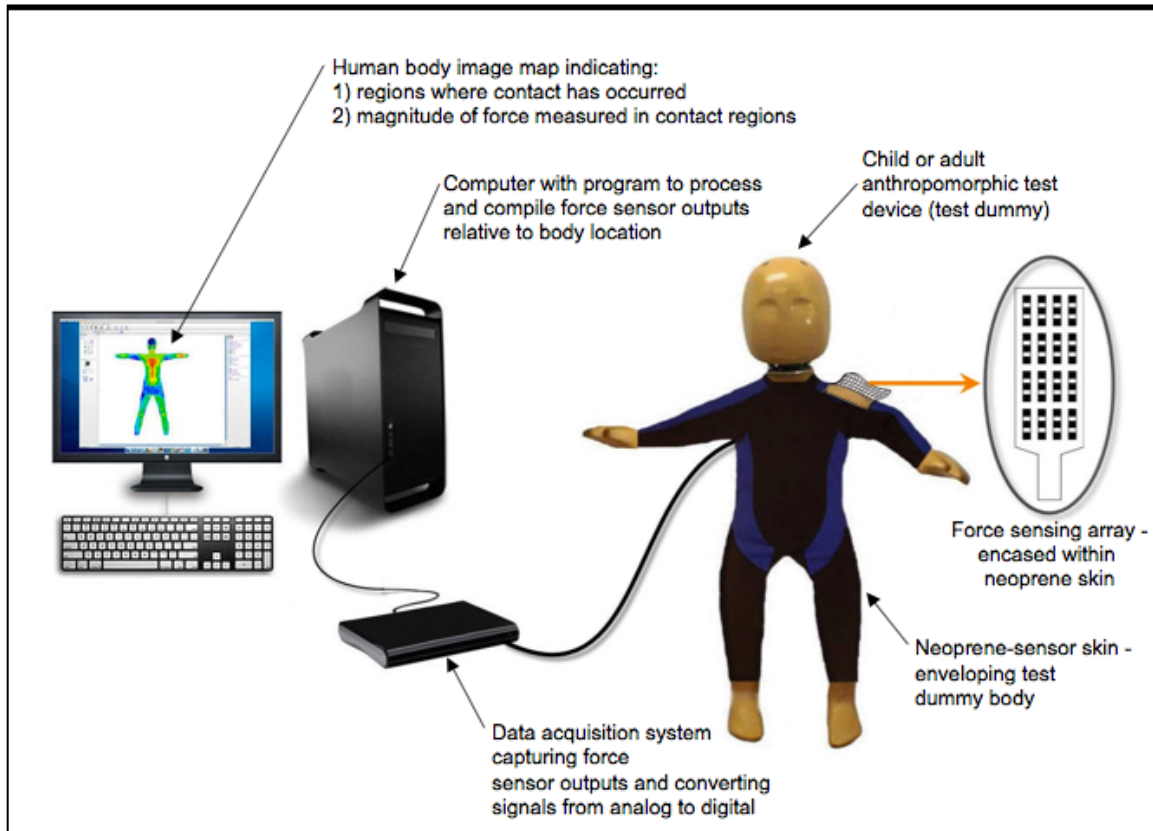


Figure 1. Conceptual model of surrogate bruising detection system
(US Patent No. US 2008/0289438 pending)

To establish a firm basis for design and development, the various methodological steps were first applied to the design and development of a forearm-only prototype. Once this prototype was complete and found to meet our design goals, the methods were re-applied and extended to the design and development for all body regions. The surrogate bruising detection system was developed specifically for the 12 month old CRABI ATD (part of our existing laboratory resources) since bruising in this age group of children who are not independently mobile is often suggestive of abuse [Maguire,

2005; Sugar, 1999] and given that there is a high rate of abuse related fatalities in children age 1 year or less.

It is important to note that the design process is almost always an iterative process as will be evident in the methods used to advance our prototype. Often initial prototypes must be developed and evaluated so as to better inform subsequent prototype development. Additionally, although an attempt was made to obtain all candidate commercial sensors at the outset of the project, some sensors were obtained once the evaluation process was underway. Thus, some testing and evaluation results did not include all sensors. Moreover, once a candidate sensor was eliminated from further consideration, it was no longer included in the evaluation process.

Sensor Evaluation

Establishment of design criteria for sensing skin – Design criteria that must be met by sensing skin prototypes were established. Design criteria included factors such as force or pressure sensing range, sensor density, sensor array spatial resolution, sensor sensitivity, % error over sensing range, response time, repeatability, flexibility of sensor body and matrix, adaptability to non-uniform geometry, sensor and matrix weight, thickness, and cost.

Evaluation of commercial sensor technologies – Commercially available distributed and discrete force sensors were evaluated against established design criteria for potential use in the sensing skin. We initially assessed the feasibility of using resistive, capacitive and optical type force sensors. A comparative characteristics matrix was generated to evaluate sensors and their ability to meet design

requirements. If commercial sensors failed to meet design criteria, in-house sensor design and fabrication would need to be explored.

Design and fabrication techniques of in-house developed sensors – Commercial customized sensor matrices (i.e. a single substrate containing multiple sensors of varying sizes and shapes) designed to adapt to contoured body regions of the ATD were found to be cost prohibitive and individual off-the-shelf commercial sensors would have led to an unacceptably high sensor density and sensing skin mass (see Results for additional details). Thus the design and fabrication of in-house developed sensors, an additional step not anticipated in our original research plan, were explored. The following methodology of producing individual force sensing resistive sensors (FSRs) was evaluated:

1. Milling of conductive patterns onto a flexible copper-coated substrate using a rapid circuit board plotter.

Given the excessive wiring necessary to interconnect individual sensors, additional methodologies were evaluated to generate an integrated matrix of sensors on a single substrate for a specific region of the ATD, thereby reducing interconnecting wiring. FSR conductive side sensor matrices were produced using:

1. Photolithography, where a matrix of individual sensor patterns were transferred from a photo mask onto a copper substrate, which was then etched to produce a desired space and trace pattern. (This technique was carried out by our research team at the University of Louisville Micro/Nano Technology Center.)

2. Printing the sensor matrix pattern directly onto flexible copper clad substrate using a solid ink (wax) laser printer, followed by a copper etching process.

Various conductive side space and trace pattern designs generated using the above in-house methodologies were coupled with semi-conductive materials to create a complete FSR. Two different semi-conductive materials having resistances of 900 K-ohm and 250 K-ohm were joined with the conductive side designs for evaluation purposes. Cabling and cabling interface strategies (between the sensor matrix and cable, and between the cable and data acquisition hardware components) were evaluated for in-house generated integrative sensor matrices.

Characterize commercial and in-house fabricated sensors - A customized data acquisition system, including a custom graphical interface program (Labview 2009; National Instruments) and associated hardware, was developed to acquire, measure, and record force application and sensor output to characterize both commercial and in-house sensors. Sensors having the greatest change in resistance for a given range of force application to the sensor surface would be capable of capturing the widest range of force application when incorporated into the sensing skin. Both static and dynamic load testing were conducted to generate characteristic sensor curves.

Sensing Skin

Incorporate sensors into protective neoprene jacket to form sensing skin – Individual commercial sensors were inserted into separate pockets of a neoprene protective layer cut so as to envelop the ATD forearm creating a prototype sensing skin. Similar sensing skin prototypes were generated using the in-house milled conductive side joined with a semi-conductive layer to create individual FSRs. In-

house generated integrated sensor matrices on a single substrate (conducted side matrix joined with semi-conductive layer) were sandwiched between two layers of neoprene cut in a pattern so as to snugly fit to the ATD's forearm.

Data Acquisition System (DAQ)

Subsequent custom data acquisition systems, linked to each of the sensors within the matrix enveloping the forearm, were developed to acquire, process, analyze, store and present sensor output when force was applied to the sensing skin/forearm. Labview Virtual Instruments (VI) were developed for this purpose and displayed a 2D sensor map and a 3D forearm image with an underlying discretized grid that paralleled the location of the individual sensors within the forearm skin. A computer display indicated both magnitude of force application, as well as location of activated sensors. Level of force application was conveyed as a color that corresponded to a pre-determined color-coded range.

Evaluation of Sensing Skin Prototypes

Prototype forearm sensing skins generated using individual sensors (3 prototype sensing skins) and integrated sensor matrices (2 prototype sensing skins) were evaluated against design goals. Overall system function was demonstrated through force application to the sensing skin and assuring that a corresponding response (force magnitude and location) was displayed on the 2D map and 3D forearm image.

Characterization of chosen sensing skin - Following selection of the sensing skin that best met our design goals, this prototype response was characterized by applying known dynamic forces to a forearm equipped with the chosen sensing skin (integrated sensor matrix produced through solid ink

printing) to generate a characteristic force vs. sensor output curve for use as a calibration curve in our data acquisition system.

Extend Sensing Skin to Entire ATD

Design patterns for each of the ATD body regions were generated and printed using the space and trace pattern found to produce the most desirable characteristic response. The design of sensor matrices were developed such that they would contour to the ATD body region producing a smooth, seamless fit when sandwiched between inner and outer protective neoprene layers. Discrete sensors that together formed an individual body region integrated sensor matrix on a single substrate were designed such that they provided a clinically relevant resolution of force application (i.e differentiation of force application location to ATD body region). Cabling was interfaced to each integrated sensor matrix, which in turn was multiplexed into a larger flat flexible cable that interfaced to the data acquisition system.

III. Results

Sensor Evaluation

Our original intent was to utilize commercially available sensors to develop our sensing skin. However, it was determined that *customized* sizes and shapes of commercial sensors joined together on a single substrate and adapted to various regions of the ATD were cost prohibitive. Customization costs were not only beyond the available project budget, but also would have led to a system that exceeded market value. Thus, we initially created a prototype(s) forearm sensing skin using off-the-shelf commercial sensors of limited available sizes and shapes.

Given that capacitive and optical sensors are typically unable to sustain impact without damage to the sensor structure, we eliminated these types of sensors from further consideration and focused our evaluation on force sensing resistive sensors (FSRs). The basic principle of these sensors is that predictable changes in resistance are produced with the application of force to its surface.

Manufacturer specifications of commercial FSR sensors along with preliminary design criteria were compiled in a matrix (Appendix A) as a first step towards comparing candidate sensors.

Commercial off-the-shelf FSR sensors available to us were statically tested to determine % error over a loading range (Appendix B). Additionally, commercial sensors showing promise based upon static testing results, along with our in-house milled copper clad conductive side joined with various semi-conductive materials to form an FSR sensor, were evaluated under impact loading conditions¹ to characterize sensor change in resistance vs. force application (Appendix C). (Figure 2 illustrates various space and trace conductive side designs. Figure 3 illustrates the implementation of these designs resulting in milled copper clad conductive side prototypes.) The finest space and trace pattern produced the most desirable characteristics (i.e. having the greatest change in resistance over a loading range), and thus was the sensor design further evaluated through impact testing (Appendix C). Semi-conductive materials with varying resistance levels were paired with our U of L milled conductive side for impact testing. It was determined that our in-house milled copper clad, finest space and trace conductive side, combined with semi-conductive material to create a force resistive sensor produced the most desirable characteristics given its capacity to discriminately sense the broadest range of force application.

¹ Impact testing consisted of dropping a pivoting hammer from known heights onto our sensor (comprised of conductive and semi-conductive layers enveloped by a neoprene layer on the top and ATD skin layer on the bottom) that was placed atop a load cell. The voltage output from the sensor and the load imparted to the load cell was collected via a data acquisition system

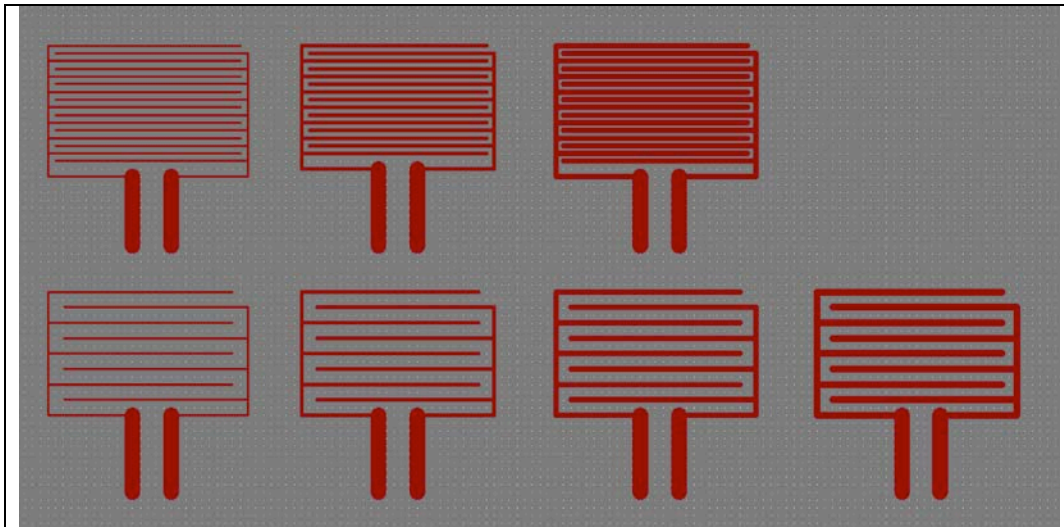


Figure 2. Conductive side space and trace designs to be implemented through milling of copper clad substrate.

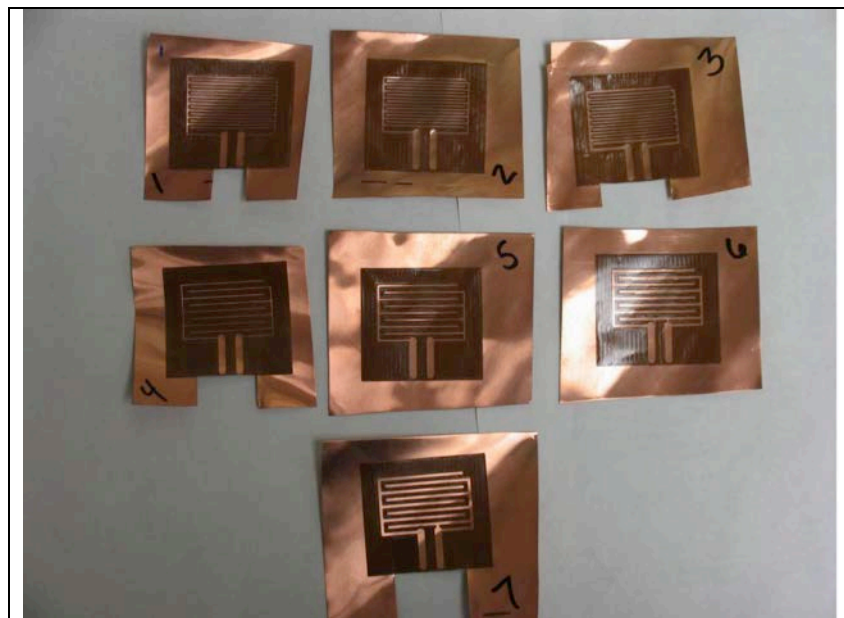


Figure 3. Milled copper clad conductive side with various space and trace patterns.

In-House Integrated Sensor Matrix Design and Fabrication

Although the copper clad milled sensors produced desirable characteristics, it was determined that individual sensors would lead to excessive wiring and thus, excessive bulk and weight in our sensing skin (see Figure 7a and 7b). Moreover, this increased bulk could potentially interfere with sensor function when sensing skins from multiple body regions were introduced. Thus, we sought to develop

a conductive side of an FSR sensor with multiple integrated sensors on a single substrate that also incorporated wiring to join the sensors. This approach would lead to a uniform thickness across the sensing matrix. Wiring for all sensors within the matrix were designed to have a common terminal point that would interface with external cabling.

A sensor matrix design incorporating eight (8) individual sensors and their associated wiring was generated for the ATD forearm (Figure 4). This matrix configuration was established with the intent of being able to wrap it, enveloped with neoprene protective layers, around the ATD forearm.

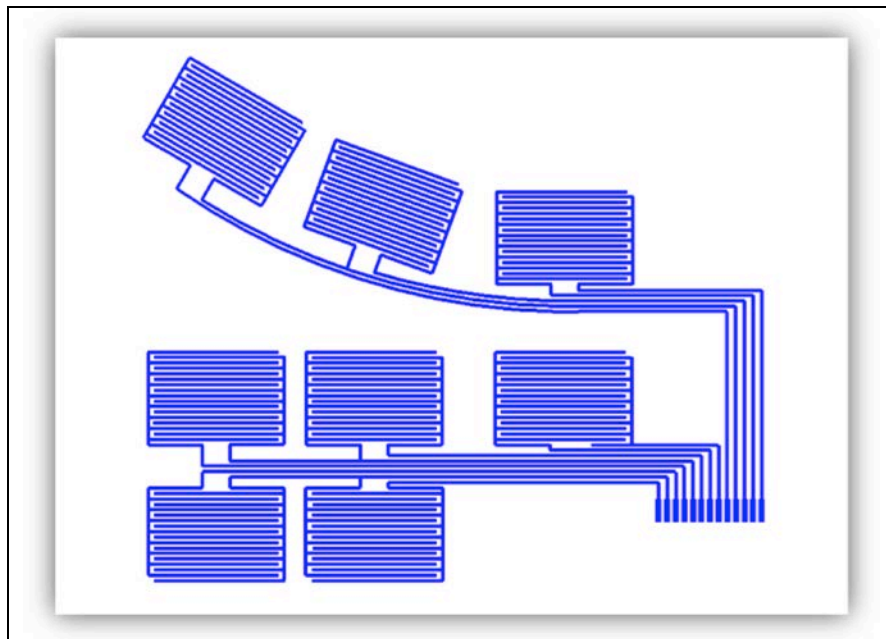


Figure 4. Drawing of forearm conductive side of integrated sensor matrix incorporating 8 individual sensors and associated wiring and terminal end connection.

To create the 8-sensor matrix design shown in Figure 4 we approached a contract manufacturer (Samtec, Inc.) to determine their capability to produce the desired prototype matrix and obtain a cost to do so. Although they were able to produce the prototype from our design drawing, the cost would be approximately \$3000 given its level of complexity. (A second quote was obtained from Pressure

Profile Systems, Inc. for designing and fabricating a sensor matrix to adapt to the ATD forearm; this cost was \$18,000 for a single discrete sensor that would contour to the surface of the ATD forearm. Additional sensors included in the matrix would increase this cost by \$4,000. Thus, the cost for a 2-sensor forearm matrix would equate to \$22,000.) Extrapolating this cost to the entire ATD, even with our providing each ATD body region integrated matrix design, would lead to a cost prohibitive sensing skin. Thus we embarked upon attempting to fabricate this forearm sensor matrix design using affordable in-house capabilities.

As stated in the Methods, two approaches were evaluated for their feasibility; 1) photolithography - typically used to transfer geometric patterns from a mask to the surface of a silicon wafer, and 2) printing the sensor matrix pattern directly onto flexible copper clad using a solid ink (wax) laser printer, followed by a copper etching process. Appendix D outlines the steps used to attempt to create the integrated sensor matrix conductive side using photolithography in the University of Louisville Micro/Nanotechnology Center (clean room). As described in Appendix D, this method was found to produce a pattern with discontinuities, and thus was deemed to be unacceptable. However, the direct printing of the conductive side pattern proved to be successful once we employed a solid ink laser printer. This method entailed direct printing of the pattern from a CAD-based drawing onto flexible copper clad sheeting fed into the printer. The copper clad sheeting with the pattern was then subjected to etching to remove unprotected copper, thereby retaining the wax-protected copper pattern (Figure 5). Following etching, microscopic examination of the copper traces were evaluated to assure continuity, and thus uninterrupted electrical conduction (Figure 6). The final step was to protect the copper traces from corrosion by overlaying them with a tin coating. Joining the conductive side with a 1 M ohm semi-conductive material formed the FSR.

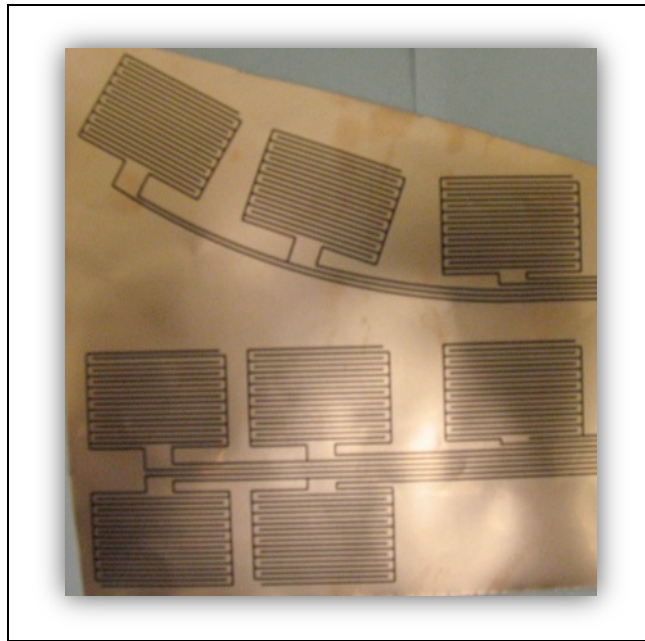


Figure 5. Conductive side forearm sensor matrix printed using solid ink on copper clad sheeting and etched.

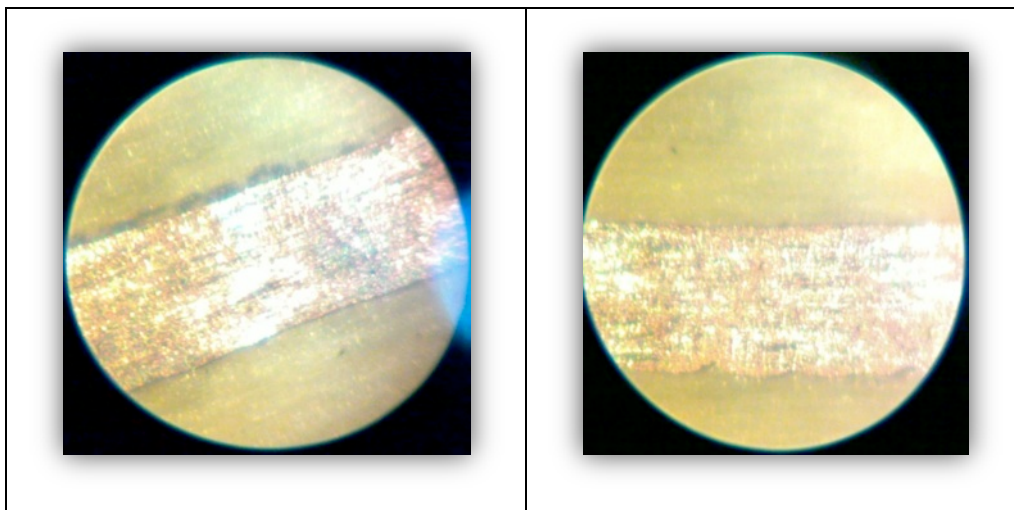


Figure 6. Microscopic images (100x) illustrating continuity of copper traces of the sensor matrix produced using the solid ink printer after etching.

In comparison to commercial fabrication of our forearm sensor matrix design (\$3000), our sensor material costs after purchasing a \$600 solid ink printer (also used to produce subsequent sensor matrices) were approximately \$20 and required approximately 4 hours for sensor fabrication.

The in-house printed sensor was compared to initially established design criteria and was determined to have acceptable performance (Appendix E).

Forearm Sensing Skin Prototypes

Forearm prototype sensing skins were generated using individual commercially available FSR sensors, as well as in-house designed and fabricated sensors. All sensors were protected by inner and outer neoprene layers cut in a pattern that fit snugly when wrapped around the forearm. Ends of the neoprene were joined together to maintain placement on the forearm. Two forearm sensing skins were developed using individual commercial sensors (Figure 7a), one forearm sensing skin was developed using individual in-house milled sensors (Figure 7b), and one forearm sensing skin was developed using an in-house printed integrated sensor matrix (Figure 7c). As evident in Figure 7, the in-house integrated sensor matrix prototype (Figure 7c) led to a sensing skin having a uniform thickness and reduced bulk. Additionally this prototype had the lowest mass, an important factor when adapting the sensing skin to the ATD so as to not alter the inertial characteristics of the ATD.

		
<p>Figure 7a. Prototype sensing skin using individual commercial sensors.</p>	<p>Figure 7b. Prototype sensing skin using individual in-house milled sensors.</p>	<p>Figure 7c. Prototype sensing skin using in-house integrated sensor matrix.</p>

In addition to the sensors having a lower mass, the cable management technique used with the integrated sensor matrix greatly contributed to mass reduction. This technique entailed soldering a ZIF

(zero insertion force) connector to the matrix terminal point, which in turn connected to a flat flexible cable (FFC).

Data Acquisition System

The FFC leading from the sensing skin prototype was interfaced directly with the data acquisition (DAQ) system to transmit sensor output. A schematic of the DAQ system is shown in Figure 8. A voltage divider circuit was introduced to convert the sensor output (resistance) to a voltage. This output voltage is proportional to the sensor supply voltage, voltage divider resistance, semi-conductive material resistance, conductive side space and trace, and applied force.

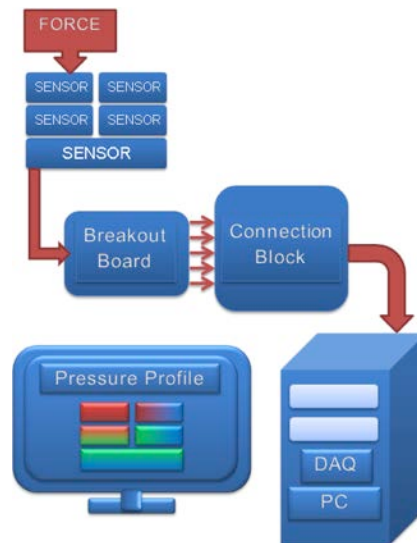


Figure 8. Data acquisition system schematic.

The performance of the prototype sensors were evaluated by applying known forces (via a materials testing machine) at varying rates as measured by a force transducer to generate a sensor voltage output vs. force application profile (Figure 9). The 100 in/min load vs. sensor voltage profile (Figure 9) was chosen as the calibration curve to be implemented in the data acquisition system given that it would more closely approximate loading experienced in a fall.

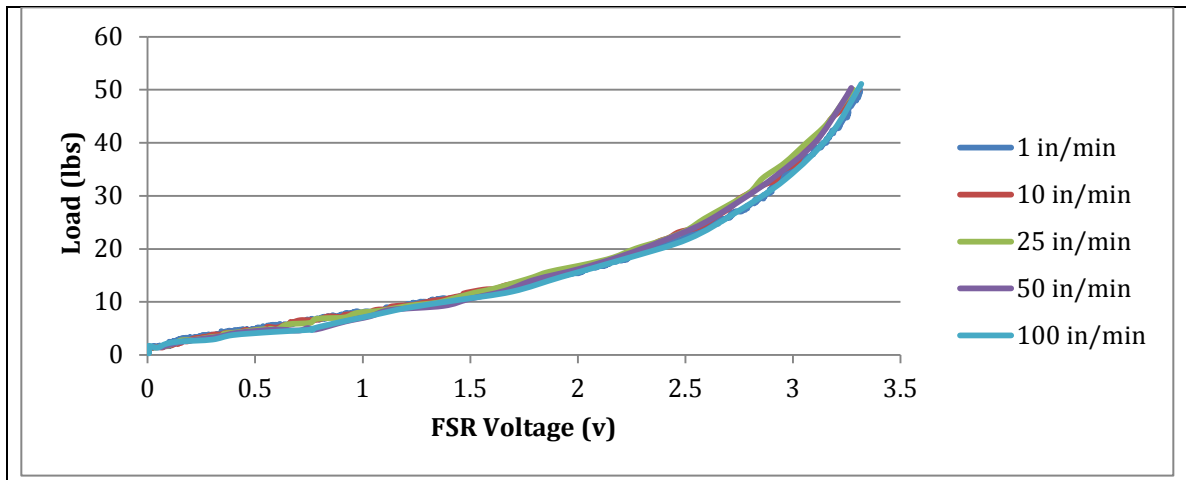


Figure 9. Load (force) vs. sensor voltage output profiles for forearm sensor at varying rates of loading.

The calibration profile was entered into the customized Labview VI developed to collect sensor data at 250,000 Hz via multifunctional DAQ boards (National Instruments; PCI-6225) that acquired, conditioned and digitized the sensor output signals within the computer. Within the Labview VI, the integrated sensor matrix output was represented on a 3D image of the ATD forearm, to provide visual details of location and active sensor value measurements. To do so, a 3D geometric solid replicating the ATD forearm was generated in SolidWorks (Dassault Systemes; computer aided design software) and imported into Labview. Within Labview, sensor output channels were discretely mapped to sensor locations and coverage areas on the 3D forearm. Once output channels were linked to their corresponding sensors, this led to an active, rotatable 3D image (Figure 10) of the forearm with color-coding indicating the level of force measured by the sensors, as well as the location of the sensor where force was applied to the forearm.

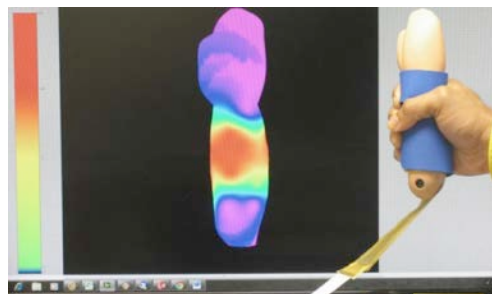


Figure 10. Demonstration of 3D forearm computer display indicating location of force application, as well as magnitude of force via a corresponding color-coded scale.

Extend Sensing Skin to Entire ATD

Integrated sensor matrices and associated wiring were designed to map to each of the remaining ATD body regions. The solid ink printing and etching technique was used to fabricate the integrated sensor matrices for each body region. Steps taken to achieve the desired forearm sensing skin prototype were repeated for each body region. Eleven (11) individual sensor matrices were designed (Appendix F) and sensing skins were fabricated to fit the head, anterior torso, posterior torso, upper arms (2), forearms (2), upper legs (2) and lower legs (2) of the ATD. Calibration curves were generated for each unique sensor design within a body region matrix and input to the data acquisition and processing system. Cabling from the various sensor matrices were multiplexed and interfaced with the DAQ system. Individual sensors within each matrix were linked to a complete 3D body image map (created by joining 3D segments of each body region developed within SolidWorks) to allow for indexing of sensor output data. The output and location of activated sensors were displayed on a 3D body image map representing the ATD. Figure 11 shows the ATD equipped with sensing skins along with the 3D body image map display.



Figure 11. Surrogate bruising detection system: ATD equipped with sensing skins and 3D body image map illustrating activated sensors.

IV. Conclusions

Discussion of Findings

Through our applied methodology we have designed, developed and fabricated a prototype surrogate bruising detection system capable of capturing and recording potential bruising patterns that occur in child surrogates used in simulated fall experiments that are often stated as false histories in child abuse. This system consists of sensing skins that adapt to a CRABI 12 month old ATD, along with a customized DAQ system and computerized 3D body map image capable of displaying the magnitude and location of force application to the ATD. Our methodology for achieving this goal differed significantly from our originally proposed plan in that we were required to design, develop and fabricate sensors for our sensing skin, whereas our original plan was to employ commercial sensors. Although this approach led to an extended project duration, we were able to develop lower cost, lighter weight sensing skins. Additionally, we have developed an effective, low cost methodology for producing customizable, lightweight force sensing resistive sensors. This low cost approach to FSR sensor development can have many additional applications.

The surrogate bruising detection system has a total of 114 sensors that cover approximately 576 square inches. This implies an approximate ATD sensor density of 0.2 sensors per square inch. The number of discrete sensing points was guided by a study that retrospectively reviewed bruising histories from the medical records of children age 0 to 48 months that had been admitted to a Pediatric Intensive Care Unit with either accidental or abusive trauma in an effort to develop a bruising clinical decision rule [Pierce 2010]. In that study, all skin findings were recorded in a skin assessment database that allowed for region-specific documentation. Each entry consisted of the type of skin finding, body region of skin finding, and the number of discrete skin findings. In our bruising detection system, we chose a sensor density to distinguish contact points on the ATD with equally distinguishable spatial resolution for the different body regions identified in the Pierce et al. study [Pierce, 2010]. Although an increased sensor density would have resulted in an enhanced resolution it would have required an increased number of sensors, connectors, and wiring; all of which would increase the weight of the bruising detection system and thus the ATD. Additionally, a higher sensor density implies an increased number of input channels to the DAQ system, thereby increasing complexity and cost.

ATDs can provide valuable data related to the biomechanical response of a surrogate human under crash conditions and have contributed greatly to assessing injury potential. However, they have been designed primarily to measure response to impacts, accelerations, deflections, forces and moments generated during a crash. ATDs do not currently have the ability to assess soft tissue injury potential such as the bruising. The goal of our system was to address the need for an ATD with the capability to assess soft tissue injury potential and record locations of impact or contact. The only comparable soft tissue injury assessment device is the Facial Laceration Measurement System (FMLS) produced by

Humanetics Innovative Solutions Inc. (Plymouth, MI). Our system differs from the FMLS in that it is capable of measuring and recording location of contact and force applied to any region of the body rather than solely the face.

Our system was designed so as to not inhibit free motion of the joints or introduce additional ATD joint resistance. This was achieved by limiting interference from the sensing skin to the moving components of the ATD. An additional goal was to assure that the inertial properties of the ATD were not altered. The total weight added to the ATD by the sensing skin over the entire surface of coverage is approximately 1.4 lbs, including all components of the sensing skin. When compared to the weight of the 12 month old ATD (22 lbs) this equates to an increase of approximately 6.4% evenly distributed over the coverage area, which should have negligible effect on ATD dynamics as it relates to inertial characteristics.

Limitations

The occurrence and severity of a bruise varies from person to person for a specific application of force given the many contributing factors that affect bruise development [Wilson 1977; Maguire 2005; Harris 2011]. Extrinsic factors such as the amount of force applied, rate of force application, the distribution of the force over larger/smaller areas, and the application of force overlying bony prominences are parameters that can affect the presence or absence of a bruise. Additionally, intrinsic factors related to the physiological and anatomical structures, such as architecture of the skin, soft tissue thickness, toughness of skin, fat content, vessel fragility, and presence and depth of underlying bone add to the complexity of this physiological event [Harris 2011]. Variables such as blood platelet levels, systemic blood pressure, vascular diseases and vasoactive or anticoagulant drug use, in addition to nutritional

and allergy related disorders can have a great influence on the presence, absence and variability of bruise intensity [Harris 2011; Kaczor 2006; Khair 2006; Langlois 1991]. This implies that the minimum load to cause bruising, the “bruising threshold” varies across individuals. However, it can be said with some degree of certainty that larger forces are associated with a greater potential for bruising. So in lieu of definitively asserting the presence of a bruise, we envision our system to be used as an investigative tool to determine the *potential* of bruising occurring to a specific body region under given loading conditions.

The biofidelity of the CRABI ATD, and in particular the soft tissue biofidelity, is a limitation of our bruising detection system. The ATD surrogate tissue consists of a heat cured vinyl plastisol which is molded to mimic the contours of the body regions. Urethane foam is sandwiched between outer and inner layers of vinyl plastisol, which is compliant and is intended to represent the soft tissue of a child. Surrogate “tissue” biomechanical properties can greatly influence force measured by our system given that the sensor-measured forces are proportional to the stiffness of the underlying ATD surrogate soft tissue. Additionally, the underlying skeletal structure and the extent or thickness of overlying soft tissue can also influence whether a bruise occurs in a child (e.g. for a given application of force bruising is more likely to occur to the shin vs. the abdomen given limited soft tissue overlying the tibia). However, the ATD “skeletal structure” relative to the skin and soft tissue thickness do not accurately represent that of a human child, and thus may influence the force measured upon contact. Similarly, we were unable to adapt sensors to the ATD joints given that our sensor matrices are unable to stretch to accommodate joint range of motion. Also, since the CRABI ATD was primarily designed for measuring a child’s response to a high deceleration automotive crash environment, testing conducted with the ATD in lower deceleration events (e.g. short distance falls) is limited by the biofidelity of the

ATD. Moreover, the CRABI ATD is not capable of replicating protective reflexes that a 12-month old may exhibit in a fall. These limitations should be taken into account when using the ATD adapted bruising detection system to assess bruising potential in falls.

Implications for Policy and Practice

When implemented in simulated falls or events, our prototype surrogate bruising detection system will have the potential to aid in determining whether a child's injuries were a result of abuse or an accident. The surrogate bruising detection system will have the potential to influence child abuse diagnosis, investigations and prosecution by providing objective biomechanical information. In the diagnosis, investigation and legal prosecution of child abuse cases, bruising patterns are often disregarded by pediatricians, child protective services, law enforcement personnel, biomechanics experts, and the judicial system given that these injuries are typically not life threatening. However, ignoring the presence of bruising patterns is a missed opportunity to gain a better understanding of the environment that a child has been exposed to since bruising provides a "roadmap" of the child's exposure to force application. The project PI (GB) has served as an expert in a number of medico-legal cases where biodynamic analysis based upon bruising patterns has provided key evidence in the prosecution of child abuse [California vs Granados, 2007; Richards, 2006]. Additionally, the project PI was a member of a child advocacy team (Pittsburgh Children Hospital) working with emergency medicine pediatricians and who together have relied heavily on bruising patterns as a factor in the diagnosis of child abuse. Use of the surrogate bruising detection system will provide a step towards equipping clinicians, child protective services, law enforcement personnel and judiciary personnel with objective data as to the bruising patterns that can be expected in common household accidents that are often provided as false histories in an effort to conceal child abuse. Conversely, use of the

surrogate bruising detection system in its ability to provide objective data regarding bruising patterns can also serve to exonerate those who are innocent of alleged abuse. In summary, the prototype surrogate bruising detection system provides an objective method to elucidate the differences in bruising patterns that can occur in abuse vs. accidents.

Implications for Further Research

A time consuming, labor-intensive challenge that we faced in our development was creating 2D substrate patterns to smoothly fit the irregular contours of the various ATD body regions. Once the pattern was manually generated, it would be recreated as a 2D CAD drawing, so as to allow for the iterative design and placement of sensors to form the matrix and associated wiring. Future efforts should include scanning 3D ATD segments and exploring options for automated 2D pattern generation through the use of software such as Autocad 123Make.

The current surrogate bruising detection system prototype consists of individual sensing skins adapted to the various ATD body regions. Subsequent prototypes will move towards integration of the individual sensor matrices into a contiguous, neoprene-protective skin. This future effort could be accomplished through working with a costume designer having sewing, pattern design and fabric selection expertise. Additionally, the 3D body map image will be migrated from a 3D adult to a 3D model of the CRABI 12-month-old ATD. An improved 3D interface allowing for zooming to regions of interest will also be explored. A telemetry or on-board data collection and recording system would reduce or eliminate cabling interference with ATD dynamics during fall experiments.

The next steps needed to advance our research in this area is to utilize the surrogate bruising detection system deployed on the CRABI ATD in fall experiments. This will allow for the development of a knowledge base of “bruising roadmaps” defining the potential bruising location and numbers associated with household falls. A knowledge base of containing this type of data can be a step towards improved differentiation between abusive and accidental in children presenting with bruising. Additionally, we will seek to verify our predicted bruising patterns against actual skin findings in children of similar age who have fallen in manner that has been documented and similar to that of our experimental falls.

V. References

- Alexander, R, Crabbe, L, Sata, Y, Smith, W and Bennett, T (1990). "Serial abuse in children who are shaken." Am J Dis Child 144: 58-60.
- America, PCA (2008). Total Estimated Cost of Child Abuse and Neglect in the United States: The Statistical Evidence. Chicago, IL.
- Atwal, GS, Rutty, GN and Carter, N (1998). "Bruising in non-accidental head injured children: a retrospective study of prevalence, distribution and pathological associations in 24 cases." Forensic Science International 96:215-230.
- Barlow, B, Niemirska, M and Gandhi, R (1983). "Ten years of experience with falls from a height in children." J Pediatric Surg 18: 509-11.
- Bertocci, G and Pierce, MC (2006). "Application of Biomechanics Aiding in the Diagnosis of Child Abuse." Clinical Pediatric Emergency Medicine 7(3): 143-8.
- Bertocci, G, Pierce, MC, Deemer, E, Aguel, F, Janosky, J, et al. (2003). "Using test dummy experiments to investigate pediatric injury risk in simulated short distance falls." Arch Pediatr Adolesc Med 157(5): 480-6.

Bertocci, G, Pierce, MC, Deemer, E, Aguel, F, Janosky, J, et al. (2004). "Influence of fall height and impact surface on biomechanics of feet-first free falls in children." Injury Prevention 35(4): 417-24.

California vs. Claudia Gabrielle Granados (2007). Criminal Case No: BB411810; Superior Court of the State of California, County of Santa Clara.

Carpenter, RF (1999). "The prevalence and distribution of bruising in babies." Arch Dis Child 80: 363-6.

Coghan, A (2005). "Science can balance the scales of justice." New Scientist. July 30, 2005: 6-9.

Cory, C and Jones, M (2003). "Can shaking alone cause fatal brain injury? A biomechanical assessment of the Duhaime shaken baby syndrome model." Med Sci Law 43(4): 317-33.

Cross, TP, Walsh, WA, Simone, M and Jones, LM (2003). "Prosecution of child abuse. A meta-analysis of rates of criminal justice decisions." Trauma, Violence & Abuse 4(4): 323-40.

de Silva, S and Oates, K (1993). "Child homicide - the extreme of child abuse." Med J Aust 158: 300-1.

Deemer, E, Bertocci, G, Pierce, MC, Aguel, F, Janosky, J, et al. (2005). "Influence of wet surfaces and fall height on pediatric injury risk in feet-first freefalls as predicted using a test dummy." Medical Engr & Physics 27: 31-9.

DHHS (2000). Healthy People 2010: Understanding and Improving Health; 2nd ed. Washington, DC, Center for Disease Control and Prevention.

DHHS (2006). Child Maltreatment 2006. Washington, DC, Administration on Children, Youth and Families.

Dsouza R, Bertocci G, (2012) "Design and development of a surrogate bruising detection system to describe bruising patterns in children." in review Forensic Science International.

Duhaime, AC, Gennarelli, T, Thibault, LE, Bruce, DA, Margulies, SS, et al. (1987). "The shaken baby syndrome: a clinical, pathological and biomechanical study." J Neurosurg 66: 409-15.

Dunstan, FD (2002). "A scoring system for bruise patterns: a tool for identifying abuse." Arch Dis Child 86:330-333.

- Harris T, Bruises and skin lesions, in: C. Jenny (Ed.) Child abuse and neglect: Diagnosis, Treatment and Evidence, Elsevier Saunders, Canada, 2011, pp. 237-251.
- Hayes, W, Erickson, M, Power, E and Gwaseob, S (2007). "Forensic injury biomechanics." Annual Review Biomed Engineering 9: 55-86.
- Herman-Giddens, M (1999). "Underascertainment of child abuse mortality in the United States." JAMA 282(5): 463-7.
- Herr, S, Pierce, MC, Vogeley, E, Zuckerbraun, N, Gaines, BA, et al. (2003a). "Auricular bruising as a marker of severe abusive trauma." Pediatr Acad Soc Conf Proc 53(4): 192A.
- Herr, S, Pierce, MC, Vogeley, E, Zuckerbraun, N, Gaines, BA, et al. (2003b). "Serious abusive trauma: an age-based comparison of presentations, injuries and outcomes." Pediatr Acad Soc Conf Proc 53(4): 124A.
- Jenny, C, Fukuda, T, Rangarajan, N, Shams, T and Bigge, RJ (2006). "Use of anatomic testing devices in modeling abusive and accidental head injuries." Pediatr Acad Soc Conf Proc: 2913.447.
- Jenny, C, Hymel, K, Ritzen, A, Reinert, S and Hay, T (1999). "Analysis of missed cases of abusive head trauma." JAMA 281: 621-6.
- Kaczor K, Pierce M, Makoroff K, Corey T, (2006). "Bruising and physical child abuse." Clinical Pediatric Emergency Medicine, 7:153-160.
- Khair K, Liesner R, (2006). "Bruising and bleeding in infants and children-a practical approach." British Journal of Haematology, 133:221.
- Thompson, AK, Bertocci, G, Pierce, MC (2009). "Assessment of head injury risk associated with feet-first free falls In 12-month-old children using an anthropomorphic test device." J Trauma 66(4): 1019-1029.
- Thompson, AK, Bertocci, G, Pierce MC, (2012). "Assessment of injury potential in pediatric bed fall experiments using an anthropomorphic test device." in review Accident Analysis & Prevention.
- Labbe, J and Caouette, G (2001). "Recent skin injuries in normal children." Pediatrics 108(2): 271-6.

- Langlois N, Gresham G, (1991). "The ageing of bruises: A review and study of the colour changes with time." Forensic Science International, 50:227-238.
- Lynch, A (1975). "Child abuse in school-age population." J School Health 45: 141-8.
- Maguire, S, Mann, MK, Sibert, J and Kemp, A (2005). "Are there patterns of bruising in childhood which are diagnostic or suggestive of abuse? A systematic review." Arch Dis Child 90: 182-6.
- Mortimer, PE and Freeman, M (1983). "Are facial bruises in babies ever accidental?" Arch Dis Child 58(1): 75-6.
- Naidoo, S (2000). "A profile of the oro-facial injuries in child physical abuse at a children's hospital." Child Abuse Negl 24: 521-34.
- Pierce, M and Bertocci, G (2008). "Injury biomechanics and child abuse." Annual Review Biomed Engineering 10: 11.1-.22.
- Pierce MC, Kaczor K, Aldridge S, O'Flynn J, Lorenz D, (2010). "Bruising characteristics discriminating physical child abuse from accidental trauma." Pediatrics, 125: 67-74.
- Prange, MT, Coates, B, Duhaime, AC and Margulies, SS (2003). "Anthropomorphic simulations of falls, shakes and inflicted impacts on infants." J Neurosurg 99: 143-50.
- Richards, PG, Bertocci, G, Bonshek, RE, Giangrande, PL, Gregson, RM, et al. (2006). "Shaken baby syndrome." Arch Dis Child 91: 205-6.
- Sedlak, AJ, Schultz, D, Wells, SJ, Lyons, P, Doueck, HJ, et al. (2006). "Child protection and justice systems processing of serious child abuse and neglect cases." Child Abuse & Neglect 30: 657-77.
- Smith, SM (1974). "134 battered children: a medical and psychological study." BMJ 3: 666-70.
- Sugar, NF, Taylor, JA and Feldman, KW (1999). "Bruises in infants and toddlers: those who don't bruise rarely bruise. Puget Sound Pediatric Research Network." Arch Pediatr Adolesc Med 153(4): 399-403.
- Sussman, SJ (1968). "Skin manifestations in the battered child syndrome." J Pediatric 72: 99-100.
- Tjaden, PG and Thoennes, N (1992). "Predictors of legal intervention in child maltreatment cases." Child Abuse & Neglect 16: 807-21.

Tush, BAR (1982). "Bruising in healthy 3 year old children." Matern Child Nurs J 11(23): 165-79.

Wedgewood, J (1990). "Childhood bruises." Practitioner 234: 598-601.

Wilson E, (1977). "Estimation of the age of cutaneous contusions in child abuse." Pediatrics, 60:750-752.

Worlock, P, Stower, M and Barbor, P (1986). "Patterns of fractures in accidental and non-accidental injury in children: a comparative study." Br Med J (Clin Res Ed) 293(6539): 100-2.

Appendix A – FSR Sensor Manufacturer Specifications and Design Criteria

Sensor Technology	Tekscan	Trossen	PPS	Sensitronics	Criteria
Sensing range (kPa)	0–517	0–1210	0–3500	0–860	≥ 0–760
Sensing range (psi)	0 – 75	0 – 175	0 – 508	0 – 125	≥ 110
Resolution (sensors per cm ²)	0.6	≥ 0.6	5	≥ 0.6	1
Sensor elements	96	1	≤ 10,240	1	-
Sensitivity (psi)	-	1.5 – 150	-	1 – 125	≥ 0 – 110
Error	11% ²	-	-	-	≤ 5%
Response time (msec)	-	1 – 2	-	1	2
Hysteresis	-	-	-	-	≤ 5%
Conformability	☐	☐	Stretch 10%	☐	6.25 cm radius
Temperature range (°C)	-	-30 to 70	-20 to 50	-15 to 200	-20 to 50
Scan rate	500 Hz ¹	-	10 kHz	-	Variable
ADC resolution	8-bit ¹	-	12-bit	-	Variable
Weight	10 gm	-	-	-	0.1 gm/sensor
Thickness (mm)	0.15 ¹	0.2 – 1.25	3	0.2 – 1.25	1
Active area (mm x mm)	203 x 76	510 x 610	407 x 508	510 x 610	Variable

Lifetime in cycles	-	$>10^6$	-	$> 10^6$	$> 50,000$
Cost	-	\$ 8.31	-	-	\leq \$ 0.50

1 - http://www.globalspec.com/FeaturedProducts/Detail/Tekscan/FScan_InShoe_Pressure_Measurement_System/4278/0 &

<http://www.bioland.com.tw/documents/tekscan/F-Scan%20Flyer.pdf>

2 - <http://www.tulane.edu/~sbc2003/pdfdocs/1073.PDF>

Note: Data was unavailable from manufacturers for some characteristics.

Appendix B – Static Loading Characterization of Commercial FSR Sensors

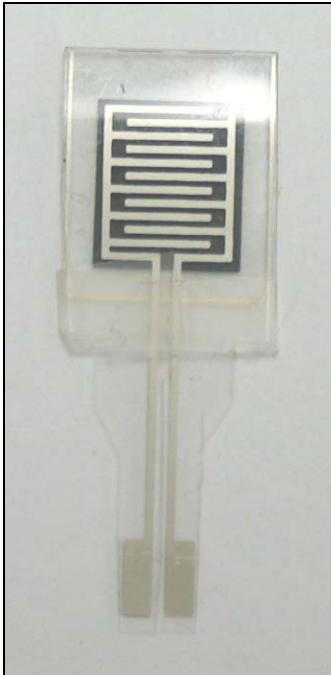
Sensitronics square sensor with spacers



- Sensor dimensions: 32 mm x 32 mm,
Thickness = 0.35 mm
- Resistance Range – 3 M ohms to
0.15 K ohms
- Sensor rise time – 0.1 sec

Static Load (lbs) over 0.75 in ²	Pressure applied (psi)	Data Acquisition Reading (psi)	% Error
0.125	0.166	0.0	100.00 %
1.000	1.330	2.0	-50.38 %
3.125	4.166	4.2	-0.82 %
5.125	6.830	6.5	4.83 %
6.125	8.000	7.8	2.50 %
8.125	10.660	10.2	4.32 %

Sensitronics small square sensor



- Sensor dimensions: 12 mm x 14 mm,
Thickness = 0.27 mm
- Resistance Range – 3 M ohms to
0.15 K ohms
- Sensor rise time – 0.1 sec

Static Load (lbs) over 0.125 in ²	Pressure applied (psi)	Data Acquisition Reading (psi)	% Error
0.125	1	0	100.00 %
1.000	8	4	50.00 %
3.125	25	28	-12.00 %
5.125	41	41	0.00 %
6.125	49	49	0.00 %
8.125	65	50	23.08 %

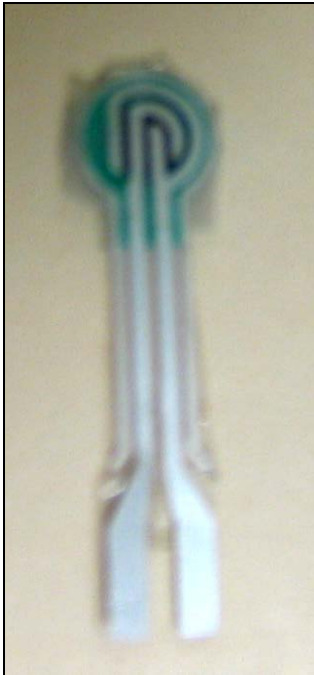
Sensitronics circular sensor with spacers



- Sensor dimensions: 35 mm dia.,
Thickness = 0.35 mm
- Resistance Range – Infinite ohms to
0.5 K ohms
- Sensor rise time – 0.1 sec

Static Load (lbs) over 0.75 in ²	Pressure applied (psi)	Data Acquisition Reading (psi)	% Error
0.125	0.166	0.00	100.00 %
1.000	1.330	2.00	-50.38 %
3.125	4.166	5.42	-30.10 %
5.125	6.830	7.00	-2.49 %
6.125	8.000	7.90	1.25 %
8.125	10.660	9.20	13.70 %

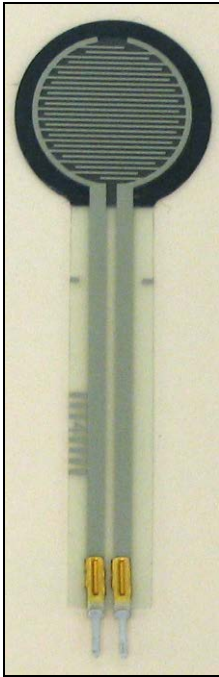
Sensitronics circular sensor small



- Sensor dimensions: 5 mm dia.,
Thickness = 0.55 mm
- Resistance Range – 6.2 M ohms to
45 K ohms
- Sensor rise time – 0.1 sec

Static Load (lbs) over 0.05 in ²	Pressure applied (psi)	Data Acquisition Reading (psi)	% Error
0.125	2.5	0	> 100.00 %
1.000	20.0	0	> 100.00 %
3.125	62.5	65	-4.00 %
5.125	102.0	55	46.08 %
6.125	122.0	110	9.84 %
8.125	162.5	140	13.85 %

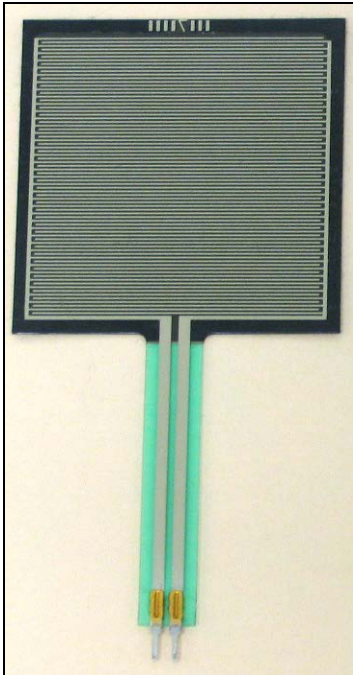
Troseen circular sensor large



- Sensor dimensions: 18.5 mm dia.,
Thickness = 0.57 mm
- Resistance Range – Infinite ohms to
0.6 K ohms
- Sensor rise time – 0.1 sec

Static Load (lbs) over 0.75 in ²	Pressure applied (psi)	Data Acquisition Reading (psi)	% Error
0.125	0.166	0.7	-321.69 %
1	1.33	3.5	-163.16 %
3.125	4.166	8.2	-96.83 %
5.125	6.83	9.4	-37.63 %
6.125	8	9.9	-23.75 %
8.125	10.66	10.6	0.56 %

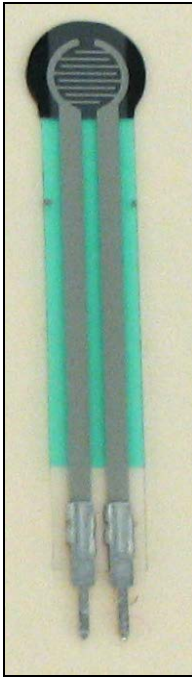
Troseen square sensor



- Sensor dimensions: 43.7 mm x 43.7 mm, Thickness = 0.57 mm
- Resistance Range – Infinite ohms to 125 ohms
- Sensor rise time – 0.1 sec

Static Load (lbs) over 0.75 in ²	Pressure applied (psi)	Data Acquisition Reading (psi)	% Error
0.125	0.166	2.2	-1225.30 %
1	1.33	4.2	-215.79 %
3.125	4.166	8.0	-92.03 %
5.125	6.83	9.5	-39.09 %
6.125	8	9.7	-21.25 %
8.125	10.66	10.5	1.50 %

Troseen circular sensor small



- Sensor dimensions: 8 mm diam.,
Thickness = 0.4 mm
- Resistance Range – Infinite ohms to
2.75 K ohms
- Sensor rise time – 0.1 sec

Static Load (lbs) over 0.12 in ²	Pressure applied (psi)	Data Acquisition Reading (psi)	% Error
0.125	1.04	1.4	-34.62 %
1.000	8.33	8.0	3.96 %
2.125	21.87	19.0	13.12 %
3.125	26.00	30.0	-15.38 %
6.125	51.00	37.0	27.45 %
8.125	67.70	37.0	45.35 %

Distance Lab square fabric pressure sensor



- Sensor dimensions: 50 mm x 40 mm,
Thickness = 4.5 mm
- Resistance Range – Infinite ohms to
4.35 K ohms
- Sensor rise time – 0.1 sec

Static Load (lbs) over 0.75 in ²	Pressure applied (psi)	Data Acquisition Reading (psi)	% Error
0.125	0.166	1.4	> -100.00 %
1	1.33	2.6	-95.49 %
3.125	4.166	2.6	37.59 %
5.125	6.83	3.0	56.08 %
6.125	8	3.0	62.50 %
8.125	10.66	3.0	71.86 %

Appendix C – Impact Testing of Commercial Sensors and In-House Milled Sensors

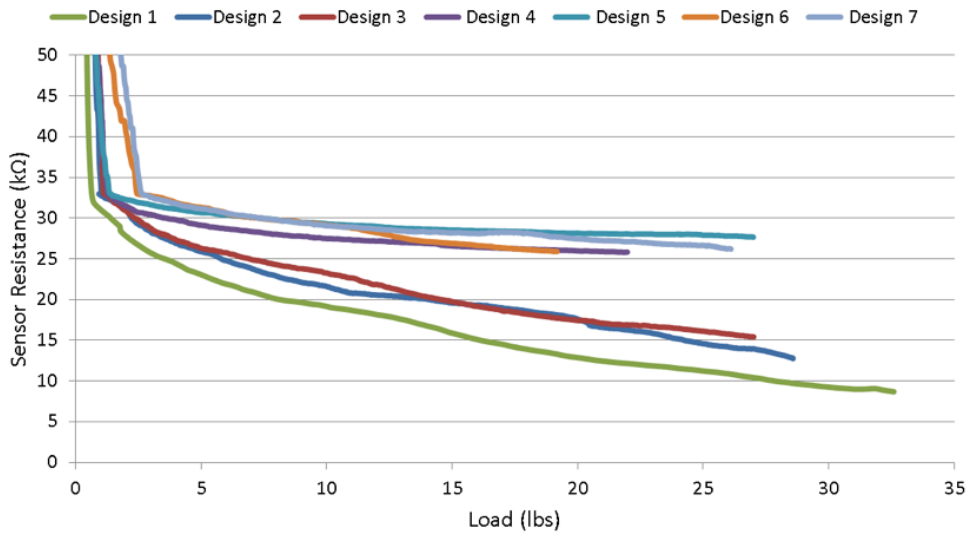


Figure C1. Dynamically applied load vs. sensor resistance profiles: in-house milled conductive side different space and trace designs joined with 500 kΩ semi-conductive material. Design 1 (green profile) represents the finest space and trace, while Design 7 (blue profile) represents the coarsest space and trace. Design 1 provided the most desirable response given its ability to output resistances that can be differentiated across the range of loads applied.

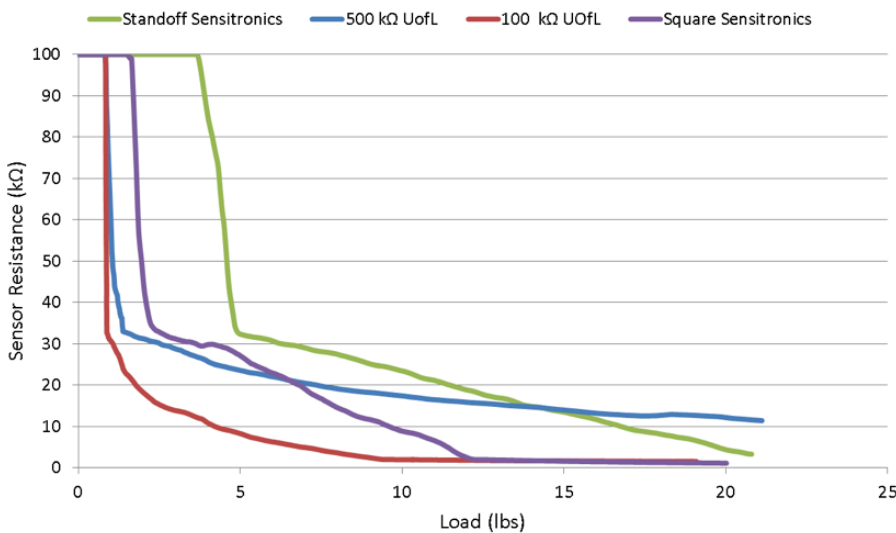


Figure C2. Dynamically applied load vs. sensor resistance profiles for select commercial FSR sensors and in-house milled conductive side (U of L; Design 1 – finest space and trace) joined with two different semi-conductive materials. The standoff spacers on the Sensitronics sensor (green profile) enabled the sensor to delay activation upon the application of load.

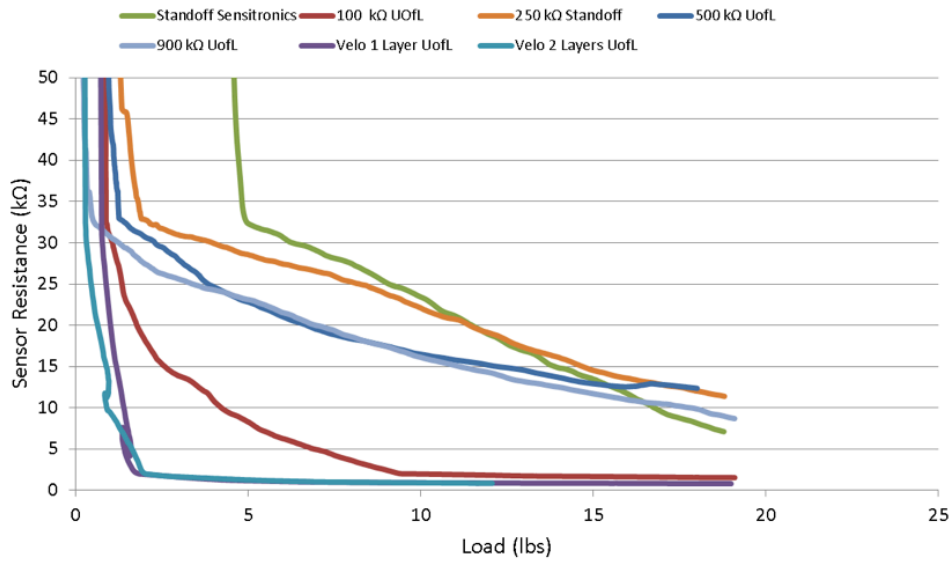


Figure C3. Dynamically applied load vs. sensor resistance profiles: semi-conductive materials evaluation when joined with in-house milled conductive side (U of L; Design 1 – finest space and trace) compared to Sensitronics (commercial) sensor with standoff spacers. The 250 K-ohm semi-conductive material produced the most desirable output given its resistance output that can be discriminated across the range of loads applied.

Appendix D – Photolithographic Process to Generate Integrated Sensor Matrix

The steps involved in the photolithographic process to create the conductive side of an FSR are as follows:

- Photomask - design and cutting - The photomask consists of a square glass plate that has a film of metal emulsion on one side. The mask is fabricated by means of an electron beam that cuts the metal layer from the glass leaving behind the shape of the design pattern (Figure D1).

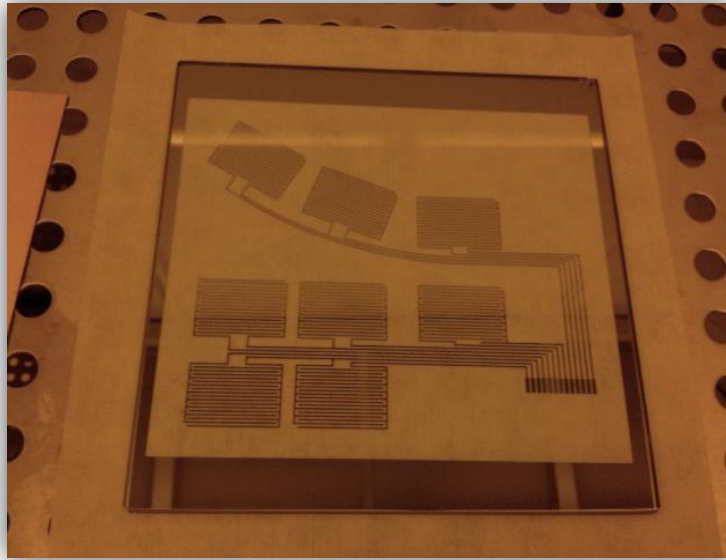


Figure D1: The glass photomask with our forearm sensor matrix pattern.

- Copper substrate – DuPont's Pyralux Copper Clad Laminate – AP9131; double sided, with a dielectric thickness of 3 mil and a copper thickness of 35 μm .
 - Cleaning – The copper substrate was cleaned with acetone to remove any waxes or oils that may be coating the surface.
 - Photoresist application - Shipley 1827 photoresist was applied to the copper substrate using the rotating process to obtain a uniform thickness (Figure D2).



Figure D2: Copper substrate positioned within rotating machine tub after application of the photoresist.

- Soft Baking – The photoresist-coated copper substrate was removed from the rotating device and placed on a hotplate at 115 degrees C for approximately 90 seconds to allow the photoresist coating film to dry (Figure D3).



Figure D3: Photoresist coated copper substrate placed on the hot plate for soft baking.

- Mask alignment and exposure – The copper substrate was aligned with and positioned beneath the photomask, and then exposed to UV radiation for 35 seconds (Figure D4). This process alters the chemical properties of the photoresist that is not protected by the photomask, thereby producing a pattern transfer from the photomask to the photoresist onto the copper substrate.



Figure D4: Glass photomask aligned over the photoresist coated copper substrate prepared for UV exposure.

- Development – The photoresistive layer on the copper substrate was developed using MF-319 developer. The copper substrate is soaked in the developer for approximately 45-50 seconds while constantly agitating the mixture (Figure D5). The substrate was examined after development to ensure that exposed photoresist has been properly developed.



Figure D5: Developing the photoresist using MF-319 developer. The copper substrate is soaked in the developer which removes the photoresist that was exposed to UV light.

- Copper Etching – The copper substrate was then placed in ferric chloride solution (FeCl_3) so as to etch away the copper that was not protected by the photoresist pattern (Figure D6). The FeCl_3 bath had to be constantly agitated and etching times varied from 120 to 150 mins.



Figure D6: Ferric Chloride used for etching the copper clad laminate in the clean room.

It is in this last step of copper etching that we experienced problems with losing portions of the protective photoresist and therefore introducing discontinuity in our pattern. We believe it is the extended time period that it takes this pattern to etch that is responsible for the intermittent loss of pattern in the photoresist. We have attempted to use various methods of reducing the pattern's FeCl exposure time with similar unacceptable results (Figure D7).

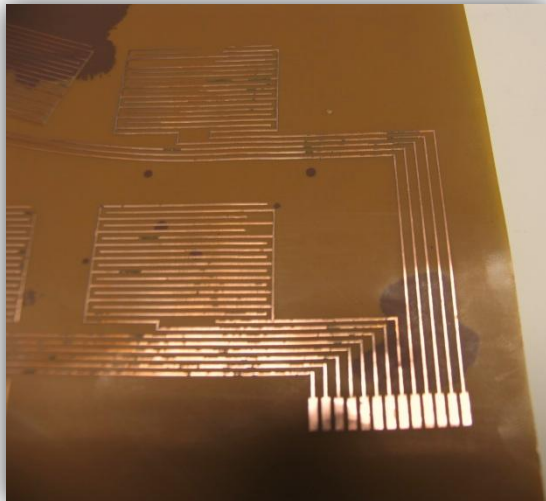
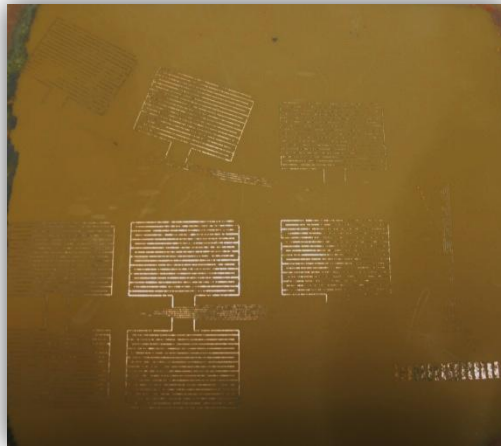
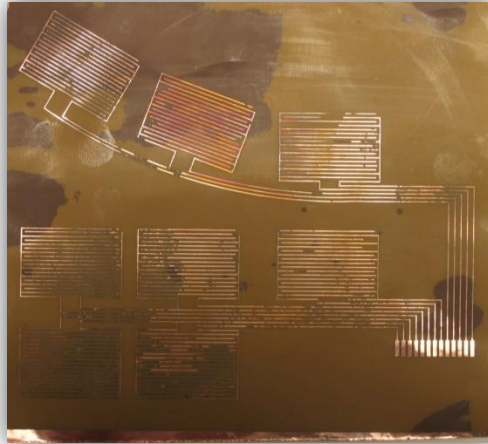


Figure D7: Various trials of etched sensor matrix patterns showing the lack of continuity in some of the traces due to under-etching of copper pattern.

Appendix E – In-House Printed Sensor Performance vs. Design Criteria

Sensor Technology	U of L Printed Sensor	Design Criteria
Sensing range (kPa)	0–690	≥ 0 –760
Sensing range (psi)	0 – 100	≥ 110
Resolution (sensors per cm ²)	>1	1
Sensor elements	Variable	-
Sensitivity (psi)	1 – 100	≥ 0 – 110
Error	-	$\leq 5\%$
Response time (msec)	≤ 1	2
Hysteresis	-	$\leq 5\%$
Conformability	6.25 cm radius	6.25 cm radius
Temperature range (°C)	-15 to 200	-20 to 50
Scan rate	250 kS/s	Variable
ADC resolution	16 Bit	Variable
Weight	0.2 gm/sensor	0.1 gm/sensor ¹
Thickness (mm)	0.3 mm	1
Active area (mm x mm)	Variable	Variable
Lifetime in cycles	$> 10^6$	$> 50,000$
Cost	\$ 0.41	\leq \$ 0.50

¹ – initially assumed greater sensor density would be desirable, but later reasoned that density could be reduced to a clinically relevant level

Appendix F – Sensor Matrix Designs for Various ATD Body Regions

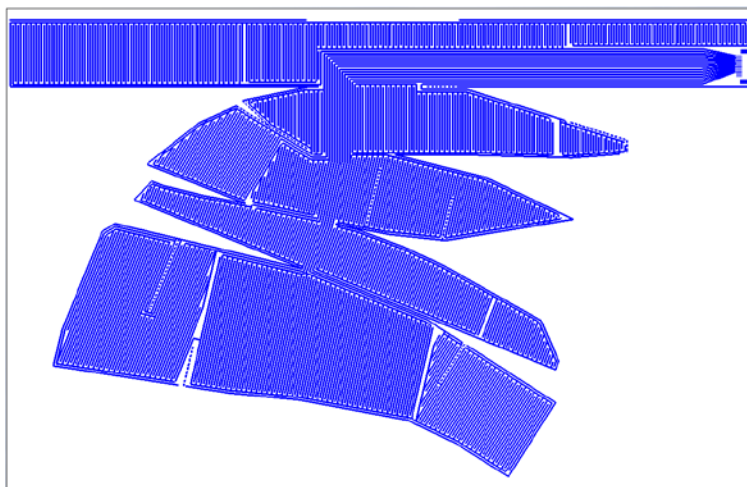


Figure E1. Head Sensor Matrix (2 each; 1 per side)

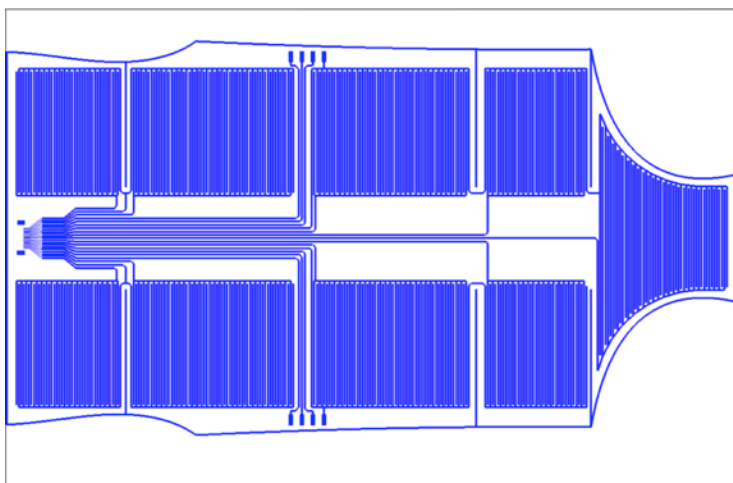


Figure E2. Posterior Torso Sensor Matrix

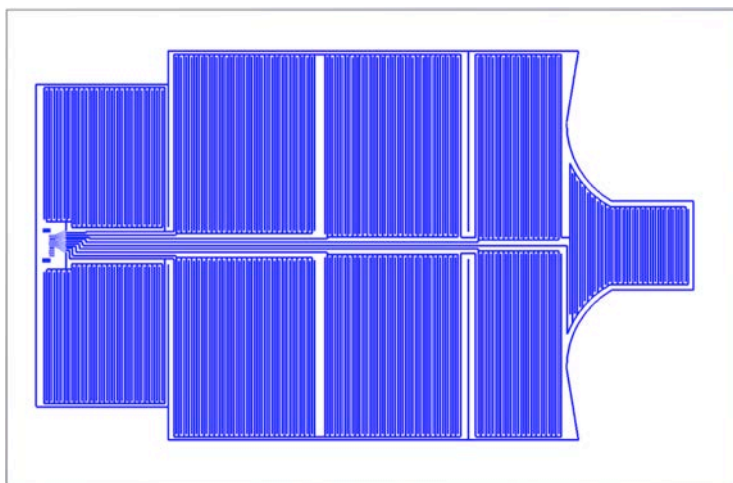


Figure E3. Anterior Torso Sensor Matrix

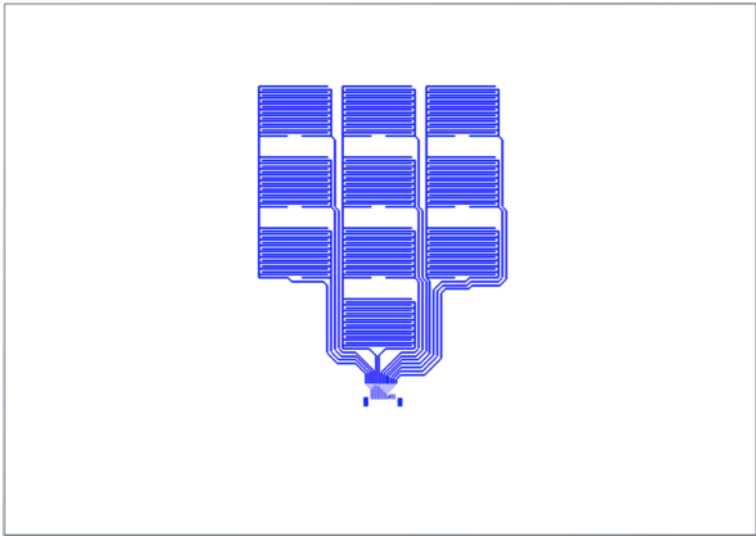


Figure E4. Upper Arm Sensor Matrix (2 each)

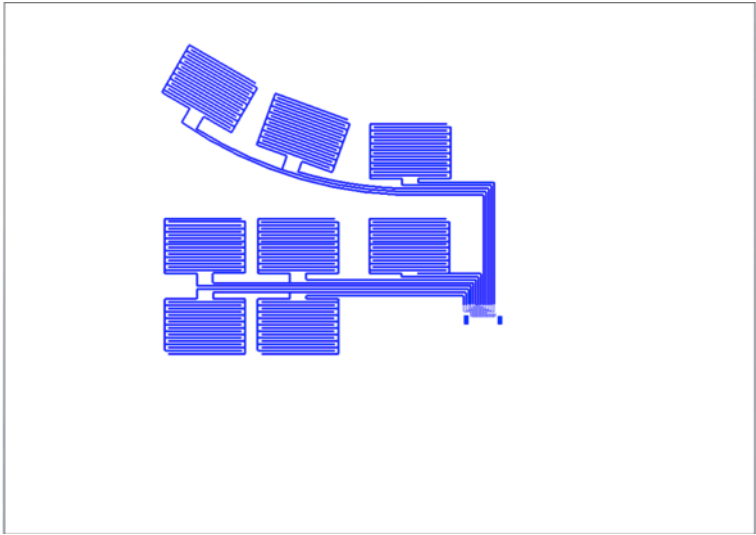


Figure E5. Lower Arm Sensor Matrix (2 each)

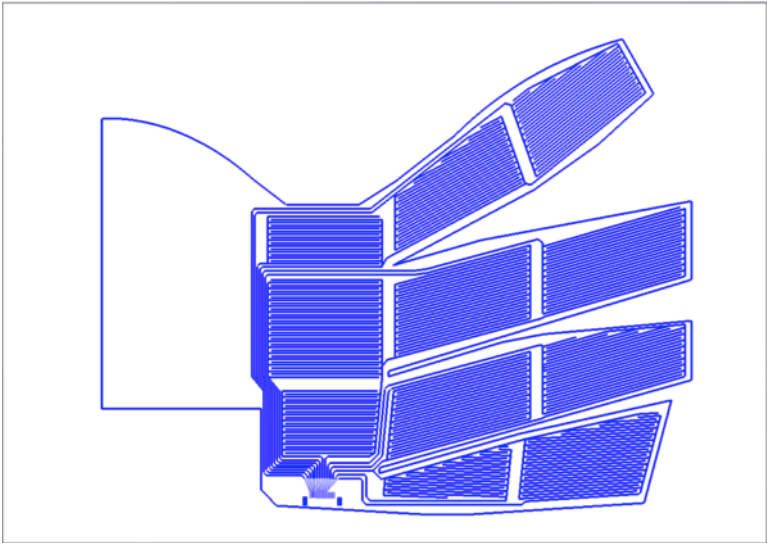


Figure E6. Upper Leg (2 each)

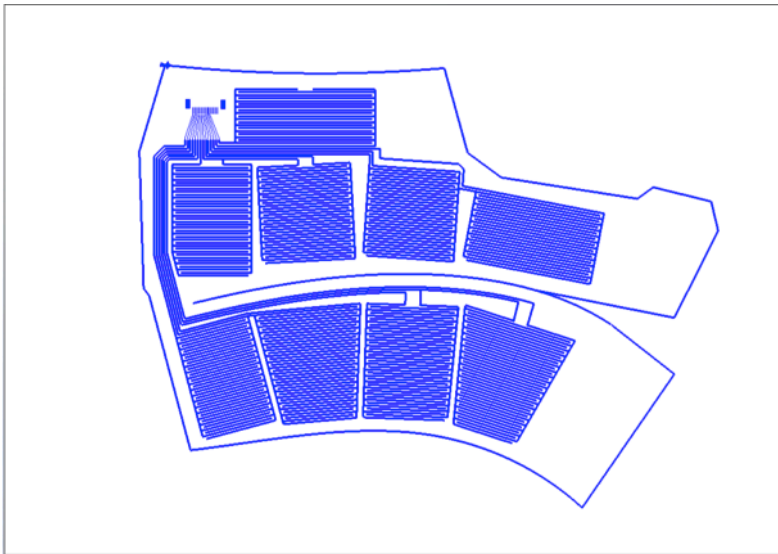


Figure E7. Lower Leg (2 each)